

**AVALIAÇÃO EXPERIMENTAL E MODELAGEM
COMPUTACIONAL DA MAGNETOFABA
ITAPUENSIS: POSSÍVEIS APLICAÇÕES EM
NANOROBÓTICA**

LUCAS FERREIRA DE MELO. DINIZ

**AVALIAÇÃO EXPERIMENTAL E MODELAGEM
COMPUTACIONAL DA MAGNETOFABA
ITAPUENSIS: POSSÍVEIS APLICAÇÕES EM
NANOROBÓTICA**

Dissertação apresentada ao Programa de Pós-Graduação em Ciência da Computação do Instituto de Ciências Exatas da Universidade Federal de Minas Gerais como requisito parcial para a obtenção do grau de Mestre em Ciência da Computação.

ORIENTADOR: OMAR PARANAÍBA VILELA NETO

Belo Horizonte
Dezembro de 2016

LUCAS FERREIRA DE MELO. DINIZ

**EXPERIMENTAL EVALUATION AND
COMPUTATIONAL MODELING OF THE
MAGNETOFABA ITAPUENSIS BACTERIA:
POSSIBLE APPLICATIONS IN NANOROBOTICS**

Dissertation presented to the Graduate Program in Computer Science of the Universidade Federal de Minas Gerais in partial fulfillment of the requirements for the degree of Master in Computer Science.

ADVISOR: OMAR PARANAÍBA VILELA NETO

Belo Horizonte

December 2016

© 2016, Lucas Ferreira de Melo. Diniz.
Todos os direitos reservados.

Diniz, Lucas Ferreira de Melo.

D585e Experimental evaluation and computational
modeling of the Magnetofaba Itapuensis bacteria:
possible applications in nanorobotics / Lucas Ferreira
de Melo. Diniz. — Belo Horizonte, 2016
xxiv, 86 f. : il. ; 29cm

Dissertação (mestrado) — Universidade Federal de
Minas Gerais

Orientador: Omar Paranaíba Vilela Neto

1. Computação — Teses. 2. Modelagem de dados. 3.
Simulação (Computadores digitais). 4. Visão por
computador. 5. Nanocomputação. I. Orientador.
II. Título.

CDU 519.6*86(043)



UNIVERSIDADE FEDERAL DE MINAS GERAIS
INSTITUTO DE CIÊNCIAS EXATAS
PROGRAMA DE PÓS-GRADUAÇÃO EM CIÊNCIA DA COMPUTAÇÃO

FOLHA DE APROVAÇÃO

Experimental evaluation and computational modeling of the magnetofaba
itapuensis bacteria: possible application in nanorobotics

LUCAS FERREIRA DE MELO DINIZ

Dissertação defendida e aprovada pela banca examinadora constituída pelos Senhores:

PROF. OMAR PARANAÍBA VILELA NETO - Orientador
Departamento de Ciência da Computação - UFMG

PROF. ERICKSON RANGEL DO NASCIMENTO
Departamento de Ciência da Computação - UFMG

PROF. LUIZ CHAIMOWICZ
Departamento de Ciência da Computação - UFMG

Belo Horizonte, 15 de dezembro de 2016.

Agradecimentos

Primeiramente devo agradecer a Deus, por ter guiado meus passos, me dando inteligência emocional e saúde para ter chegado até aqui.

Sou muito grato pela educação que me foi dada pelos meus pais. Mãe, obrigado por ter sido exemplo de estudo e dedicação, desde quando me fazia estudar numa máquina de costura até hoje, quando te acompanho virando noites no computador preparando material para a escola. Pai, obrigado por ser a razão e a diversão, que nunca me deixou titubear e sempre esteve presente nos cuidados do dia-a-dia. O mestrado representa o ápice do trabalho que vocês fizeram comigo por mais de 27 anos.

Carol, minha esposa, obrigado pelo suporte, paciência e compreensão nessa etapa tão importante. Se cheguei até aqui foi por que tive você ao meu lado, escutando as lamentações sobre o texto ou sobre os experimentos terem dado errado. Obrigado também por ter me dado mais uma família que também foi muito importante nessa caminhada. Obrigado Maria Helena, Luiz, Marina e Bernard.

Sou muito grato também à minha irmã Marcela, que se tornou um exemplo de perseverança para mim. Descobriu seu caminho por conta própria, sem medo de errar e hoje tenho certeza que ela não precisa de ninguém ditando suas escolhas.

Meu orientador Omar teve um papel muito importante nesse trabalho e nesse período de muito aprendizado. Obrigado pelos direcionamentos durante esses dois anos, por ter compreendido minha situação de mudança e por ter me ajudado muito, principalmente nos últimos seis meses.

Não posso deixar de agradecer aos amigos e colegas de Cadence, duas pessoas em especial. Andréa, obrigado pelo suporte nesse período e por ter me ajudado a ser uma pessoa melhor, tanto pessoal quanto profissionalmente. Breno, obrigado por estar sempre disposto a ajudar, pela presença constante e por ser uma referência intelectual para mim.

Finalmente devo agradecer à instituição UFMG pela excelência em educação, desde minha graduação ao mestrado. O conhecimento aprendido durante os mais de

sete anos aí dentro foi essencial em todas minhas conquistas.

“If I have seen further it is by standing on the shoulders of Giants.”
(Isaac Newton)

Resumo

A criação de nanomáquinas autônomas é um dos maiores desafios da nanotecnologia. O desenvolvimento desse tipo de robô utilizando novos materiais é promissor, porém essa abordagem não é a mais adequada quando sua aplicação está dentro do domínio biológico, devido à potencial presença de componentes nocivos à saúde. Além disso, o controle desses robôs é outro desafio, já que na escala nanométrica as leis da física se comportam diferente devido à influência da relatividade. Por essas razões, considera-se a utilização de bactérias magnetotáticas (MTB) como base para a criação de nanorobôs. Devido ao seu pequeno tamanho, característica única de se orientar por meio de campos magnéticos e por possuir um motor biológico, elas são excelentes candidatas para serem utilizadas em diversas aplicações. O problema é que existe um número relativamente baixo de culturas desses micro-organismos, o que faz com que os experimentos sejam difíceis de serem executados. Neste trabalho nós apresentamos avaliações experimentais e um modelo computacional de uma nova espécie descoberta: a *Magnetofaba itapuensis*. Encontrada na Lagoa de Itaipu, próxima à cidade do Rio de Janeiro, Brasil, a espécie é estudada e cultivada pelos pesquisadores da Universidade Federal do Rio de Janeiro (UFRJ). Ao contrário das outras espécies disponíveis, essa se move em direção ao Sul e é mais rápida. Mesmo assim, experimentos que utilizam essas bactérias são difíceis de serem realizados devido ao fato delas serem microaerofílicas, o que as faz sensíveis às altas concentrações de Oxigênio. Um microscópio e uma montagem eletrônica foram desenvolvidos para a realização dos experimentos. O microscópio montado permite a captura de imagens em diferentes resoluções e a montagem eletrônica é capaz de modificar o campo magnético sobre a amostra utilizando uma interface com o computador. Baseado nos resultados obtidos, um modelo computacional da bactéria foi desenvolvido e validado. Este modelo é aplicado para simular o comportamento da bactéria, vislumbrando possíveis utilizações do enxame de bactérias em experimentos de nanorobótica. Para tanto, um controlador *fuzzy* foi desenvolvido para o controle da posição do enxame. A ideia é desenvolver e validar o controlador em um ambiente de simulação antes de ser aplicado nas bactérias reais. O simulador é flexível, possibili-

tando a adição de novos modelos e controladores facilmente. Os resultados mostram que a espécie *Magnetofaba itapuensis* não suporta mais de 10 minutos depois de ser exposta ao Oxigênio. Com a validação do simulador os melhores parâmetros para cada modelo foram obtidos de forma a garantir um comportamento o mais próximo possível do observado nos experimentos. Considerando os modelos e seus parâmetros, as características do controlador também são avaliadas. O desenvolvimento do simulador facilitará as pesquisas nessa área, especialmente devido à dificuldade de condução de experimentos com bactérias reais, além de contribuir para um melhor conhecimento das características do sistema controle-bactéria.

Palavras-chave: Nanorobótica, Bactéria Magnetotática, Simulação, Nanotecnologia, Controle.

Abstract

The creation of autonomous nanomachines is one of the biggest challenges in nanotechnology. The creation of such robot using novel nanomaterials is promising but this approach is not recommended when the application is in the biological domain, due to the potential presence of toxic components. Besides this, controlling such robot is another challenge because in the nanometer scale the physics laws start behaving differently due to relativistic effects. For these reasons, the application of the magnetotactic bacteria (MTB) is being studied as the basis for the creation of nanorobots. Due to their small size, unique capability to orient according to magnetic fields and biological engine system they are a good candidate for several applications. The problem is that there is a relatively low number of cultures of such microorganism, making experiments hard to perform. In this work we present experimental evaluations and a computational model of the newly discovered species, the *Magnetofaba itapuensi*. This species was found in the Itaipu Lagoon near Rio de Janeiro, Brazil, and it is studied and cultivated by the researchers of the Universidade Federal do Rio de Janeiro (UFRJ). Differently from the other available species, this one has a South seeking behavior, is faster and has a coccus morphology. Even then, experiments using the bacteria are hard to perform due to their microaerophile characteristic, which makes them sensible to high Oxygen concentrations. A microscope and a computer controlled electronic setup were created to perform the experiments. The assembled microscope allows to capture images using different resolutions and the electronic system is capable to change the magnetic field over the bacteria through a computer interface. Based on the obtained results a computational model of the bacteria was created and validated. This model is applied in order to simulate the bacteria behavior, glimpsing the application of bacteria swarm in robotics experiments. For that, a Fuzzy controller was developed to control the bacteria swarm position. The idea is to test and validate the controller in a simulation environment before the tests using real bacteria. The simulator is flexible, allowing new bacteria models and controllers to be added easily. The results show that the *Magnetofaba itapuensis* species does not last longer than 10

minutes after exposed to Oxygen. With the simulator validation the best parameters of each model were obtained in order to get a simulation as close as possible to the real behavior. Considering the models and parameters, the controller characteristics were also evaluated. The development of the simulator will facilitate the research in this area, specially due to the difficult in conducting real experiments, besides contributing on the knowledge leverage of the control-bacteria system.

Palavras-chave: Nanorobotics, Magnetotatic Bacteria, Simulation, Nanotechnology, Control.

List of Figures

2.1	<i>Magnetospirillum gryphiswaldense</i>	6
2.2	Schematic of the oxic-anoxic interface (OAI)	6
2.3	<i>Magnetofaba itaipuensis</i>	7
3.1	Experiment Setup	14
3.2	Picture of the final setup	14
3.3	Coil used in the experiments	15
3.4	Top view of the board	16
3.5	Schematic of circuit to manual change the magnetic field	16
3.6	Schematic of circuit to change the magnetic field using the computer interface	17
3.7	Picture of the electronic board and the computer interface module	18
3.8	Dragonfly camera configuration window	19
3.9	Dragonfly record window	20
3.10	Simulator architecture	21
3.11	Magnetic field with coils with magnetic field on the same direction	25
3.12	Magnetic field with coils with magnetic field on opposite directions	26
3.13	Magnetic field lines generated by the script	27
3.14	Process to use the real magnetic field data on the simulator	27
3.15	Open loop approach using magnetic field gradient	28
3.16	Closed loop approach using Fuzzy controller	29
3.17	Block diagram of a Fuzzy controller	29
3.18	Membership functions	30
3.19	Result of the inference process	31
3.20	Main GUI of the simulator	32
3.21	Constrained simulation	33
3.22	Simulation using real experiment image as initial setup	33
3.23	Initial setup extraction process	35
3.24	Step input applied to the coils	36

3.25	Step response of the bacteria	36
3.26	Process to evaluate bacteria activity	37
3.27	Optical flow calculation	38
3.28	Optical flow for experiment and simulation	39
3.29	Flow histograms	40
3.30	Difference calculation procedure	41
3.31	Baseline and difference calculation for a single experiment	44
3.32	Difference calculations in two difference simulations	45
3.33	Best line slope procedure	45
3.34	Simulation enhancements flow	46
4.1	Image using 100x objective	48
4.2	Image using 100x objective containing unexpected bacteria	49
4.3	Magnetic field using the electronic system	49
4.4	Images captured using 10x and 100x objectives	50
4.5	Expected bacteria formation applying different magnetic fields	51
4.6	Calibration ruler	52
4.7	Captured image using calibration ruler	53
4.8	Step response of the bacteria	54
4.9	Activity analysis	55
4.10	Activity analysis over time	56
4.11	Activity analysis on experiments with different exposure times	57
4.12	Activity analysis on different experiments	57
4.13	Average activity and frame with maximum activity	58
4.14	Overall average difference with the different bacteria models	59
4.15	Basic model line slope analysis	60
4.16	Adapted model line slope analysis	61
4.17	Simulation agglomerating bacteria	62
4.18	Bacteria swarm control	64
4.19	Distance from swarm's center and setpoint with the different models	65
4.20	Dispersion of the swarm with the different models	65
B.1	Computer vision output	76
B.2	Image capture process	76
B.3	2D Gauss distribution	77
B.4	Line representation in the image space	77
B.5	Line representation in the parameter space	78

B.6	Different parameter conversion	78
B.7	Line representation in the parameter space using ρ and θ	79
B.8	Example of the Aperture problem	81
B.9	Magnetic Field distribution	83
B.10	<i>Biot-Savart Law</i> applied to a wire	84
B.11	<i>Biot-Savart Law</i> applied to a coil	84
B.12	RGB histogram of an image	85

List of Tables

4.1	Camera Calibration	53
-----	------------------------------	----

Contents

Agradecimientos	ix
Resumo	xiii
Abstract	xv
List of Figures	xvii
List of Tables	xxi
1 Introduction	1
1.1 Motivation	2
1.2 Overview	2
1.3 Goals	3
1.4 Structure of this work	3
2 Background and Related Work	5
2.1 Magnetotatic Bacteria	5
2.1.1 <i>Magnetofaba itaipuensis</i>	7
2.2 Nanorobotics challenges	7
2.3 Magnetotatic Bacteria usages	8
3 Methodology	13
3.1 Physical Setup	13
3.2 Microscope	13
3.2.1 Electronics	15
3.2.2 Procedures	18
3.3 Simulator	19
3.3.1 Data	21
3.3.2 Bacteria	21

3.3.3	Bacteria Models	22
3.3.4	Magnetic Field Models	24
3.3.5	Controllers	27
3.3.6	Simulation Setup	31
3.4	Analysis Tools	34
3.4.1	Bacteria Step Response	34
3.4.2	Activity Evaluation	36
3.4.3	Difference Estimation	37
3.4.4	Data Analysis	40
3.5	Model Evaluation Process	42
4	Experiments and Results	47
4.1	Real Bacteria Experiments	47
4.1.1	Setup test and evaluation	47
4.1.2	Swarm observation and electronic circuit test	48
4.1.3	Swarm observation	50
4.1.4	Camera calibration and step response	52
4.2	Activity Analysis	53
4.3	Simulator Validation	58
4.3.1	Best Model Identification	58
4.3.2	Best Parameters Identification	59
4.4	Simulator Experiments	60
5	Conclusions and Future Works	67
	Bibliography	69
	Appendix A Microscope Setup	73
	Appendix B Background review	75
B.1	Computer Vision	75
B.1.1	Image Processing	75
B.1.2	<i>Hough Transform</i>	77
B.1.3	Optical Flow	79
B.2	Magnetic Field	82
B.2.1	<i>Biot-Savart Law</i>	83
B.3	Quadratic-Chi Histogram Distance	84

Chapter 1

Introduction

Nowadays everything is connected: the phone is connected to the watch, which tracks the user's pulse sending the information over the internet. If we consider a much smaller scale (such as nanometers) the currently available devices are not capable of transmitting/receiving information. "At this scale, a *nanomachine* is defined as the most basic functional unit, integrated by nano-components and able to perform simple tasks such as sensing or actuation" [Akyildiz and Jornet, 2010].

The idea of having a *nanomachine* capable to access places never reached before is seen in many scientific fiction stories. In 1966, the movie "Fantastic Voyage" presents the idea to travel inside the human body, exploring the called "unknown universe" with the objective of repairing a brain damage [Asimov, 2011].

In the novel "Prey", by Michael Crichton (same author of "Jurassic Park"), researchers create a nanorobot capable of capturing images inside the human body and with the ability to organize themselves into a single entity, a swarm. This would make the system robust and capable to perform amazing tasks [Crichton, 2002].

Thus, in this scale there are two concepts envisioned to communicate nanomachines: one using molecular communication and another electromagnetic communication. The first aims to encode the information in molecules, which size already provides a close approach to the scale, while the later expects to use the electromagnetic radiation to exchange information [Akyildiz and Jornet, 2010].

Inside the molecular concept we can find the magnetotactic bacteria (MTB) which are micro organisms that move guided by a magnetic field. They may be used to work as *nanomachines* to perform actions human beings cannot do, such as transporting drugs inside the body, moving micro objects and also sensing (pollution, glucose level, etc).

1.1 Motivation

As said before, there are many challenges when dealing with the robotics in the nanometer scale. The same approach used in the macro scale does not apply and thus it is necessary to study new ways to perform actions and communicate. Considering the characteristics of the magnetotactic bacteria, it is possible to envision a system capable of controlling their movement.

The employment of such microorganisms as a nanorobot opens many new opportunities. First of all, it is important to highlight that they do not require any “fuel” as they use their own biomotor with high energy efficiency to move [de Lima et al., 2013]. Besides that, as an organic robot it may be easier to replicate and modify its behavior changing its DNA.

As applications, it is possible to mention the capability of transporting drugs inside the human body, sensing and performing actions in the nanoscale using a bacteria swarm. In the future it may be even possible to use them to sensor every vital signals in the body and identify any variations that may indicate diseases.

Considering the current state of the art regarding the application of magnetotactic bacteria as nanorobots, it is presented in this document an investigation of the *Magnetofaba itaipuensis* species and the development of a simulator focused on replicating the real bacteria behavior to auxiliate in future projects.

1.2 Overview

Considering that the bacterium moves according to the magnetic field direction it is possible to conceive a simple feedback loop to control such entity. In this system, the bacteria swarm position may be obtained using computer vision algorithms based on microscope images. This information is then passed to the controller which changes the tension applied to coils, varying the magnetic field around the sample, closing the loop.

But there are some problems with dealing with such bacteria: they are hard to obtain and they are microaerophile or anaerobic, which means that they die when in contact with high Oxygen concentrations [Bazyliński et al., 1994]. Considering this, experiments with them are hard to perform and do not provide much time to build and test a control system.

Therefore, it becomes necessary to model and simulate the system before performing the tests. In the simulation, each bacterium is modeled so that the model equations represent the movement of the bacterium regarding the magnetic field ap-

plied to it. Having the bacteria modeled, it becomes possible to implement and test controllers to be used in the real experiment.

1.3 Goals

This project started after some other experiments performed in the Nanocomp laboratory, which aimed to observe the connection between the behavior of the magnetotactic bacteria *Magnetospirillum gryphiswaldense* and the magnetic field direction [de Lima et al., 2013].

In this thesis, the main objective is to perform experiments using another magnetotactic bacteria species, the *Magnetofaba itaipuensis*, and implement a tool to simulate their behavior. This would make it possible to implement and validate the control system in a simulation environment.

As specific objectives there are a couple of questions to answer:

1. What is the best setup to capture the bacteria images?
2. How to control such organisms?
3. How to model and validate the bacteria behavior in the computer?
4. What is the relation between the time the bacteria is exposed to Oxygen and the observed activity?
5. The bacteria are hard to obtain, thus is it possible to prepare the experiments beforehand?

1.4 Structure of this work

In the Chapter 2 it is presented a brief background review and the state of art of using such micro organism.

The methodology used is described in the Chapter 3, including the procedures used during the experiments and the strategies to create the simulator.

In the Chapter 4 the results of the experiments using the *Magnetofaba Itaipuensis* are shown, together with the Simulator validation. The experiments are described chronologically, showing the find outs in each one. The results of the simulator validation are used to define the best bacteria computational model to use during the simulations.

Finally, Chapter 5 presents the conclusions of this thesis and discusses some possible future works.

Chapter 2

Background and Related Work

In this chapter, some background information necessary to understand this thesis are provided. The related work is presented to understand how this thesis contributes to the state of art.

2.1 Magnetotatic Bacteria

Magnetotactic bacteria are a group of microorganisms that passively align to a magnetic field as they move. This ability is due to the presence of intracellular structures called magnetosomes, which are made of magnetic iron minerals such as *magnetite* (Fe_3O_4) and *greigite* (Fe_3S_4) [DeLong et al., 1993].

These microorganisms were first documented in the early 1960's and on the following decade the terms magnetotaxis and magnetotatic started to be used for the phenomena and the bacteria, respectively. Because of the difficulties to cultivate these bacteria in laboratory and isolate them in pure culture, research in this area has been very slow. The discovery of the magnetotatic bacteria had impacted in many research fields including microbiology, geology, mineralogy and biomineralization, crystallography, chemistry, biochemistry, limnology and oceanography, physics, and astrobiology [Yan et al., 2012].

There are many species of magnetotatic bacteria varying size, format and structure of movement (cilia or flagella). Their size varies from 1.5 to $4\mu m$ and swim speed between 40 and $80\mu m/s$ [de Lima et al., 2013]. Figure 2.1 shows a bacteria of type *Magnetospirillum gryphiswaldense*. Notice the flagella on the extremities and the magnetosome in its nucleus.

Almost all species of magnetotactic bacteria are microaerophiles [Bazyliniski et al., 1994], which means they need Oxygen but they are poisoned by high concentrations of

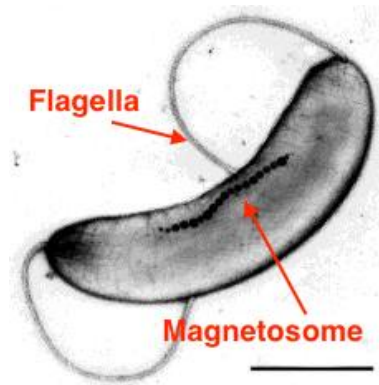


Figure 2.1. *Magnetospirillum gryphiswaldense*. Note the flagella on the extremities and the magnetosome inside the cell [Kimball, 2011].

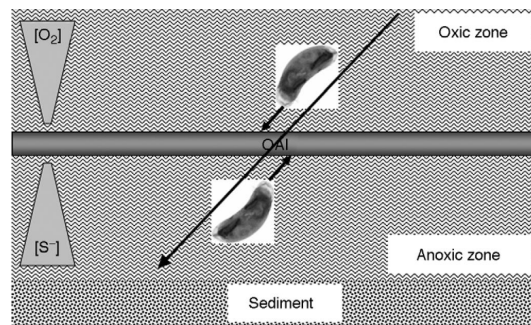


Figure 2.2. Schematic of the oxic-anoxic interface (OAI). The big arrow represents the Earth's magnetic field while the small ones represent the direction of the bacteria to maintain themselves in the OAI. The deeper the water column the lower the O_2 and higher S^- the concentrations. [Bazylinski and Schübbe, 2007].

it, or anaerobic, that do not need Oxygen and die in presence of it. Because of that, they are generally found in the anoxic regions of the habitat and in the oxic-anoxic interface (OAI), a relatively thin microaerobic zone within water columns or sediments with vertical chemical stratification, as shown in Figure 2.2.

The OAI occurs in the water column due to an inverse concentration gradient of O_2 from air at the surface and H_2S from the reduction of sulfate by sulfate-reducing bacteria present in the sediment and in the anoxic region of the water column. Cells of magnetotactic bacteria align and swim along the Earth's geomagnetic field lines, shown as the small arrows in Figure 2.2, and use chemotaxis to locate and maintain position at an optimal O_2 concentration [Bazylinski and Schübbe, 2007].

According to Silveira and Lins 2007, the culture of the magnetotactic bacteria in laboratory is really hard and only few species could be successfully maintained in a pure culture.

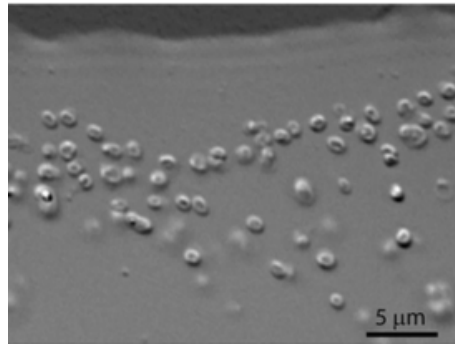


Figure 2.3. *Magnetofaba itaipuensis*

Magnetofaba itaipuensis. Note the coccus and ovoid format [Morillo et al., 2014].

2.1.1 *Magnetofaba itaipuensis*

Differently from the *Magnetospirillum gryphiswaldense*, the *Magnetofaba itaipuensis* possess a South-seeking behavior. It represents the first culture of such kind of MTB in the Southern hemisphere. Collected in the Itaipu Lagoon, in Rio de Janeiro - Brazil, the bacteria have a coccoid to ovoid morphology and are microaerophiles, meaning that they need Oxygen to survive, but in lower concentrations than the present in the atmosphere. Note in Figure 2.3 the morphology of the *Magnetofaba itaipuensis* bacteria [Morillo et al., 2014].

According to Morillo et al. 2014, another important difference between these species is the speed of the movement. The *Magnetofaba itaipuensis*, whose average size is $1.4\mu\text{m}$, has an average velocity of $186\mu\text{m}/\text{s}$ reaching up to $300\mu\text{m}/\text{s}$. This way, though their sizes are similar, this bacteria can reach almost thrice the speed of the *Magnetospirillum gryphiswaldense*.

As explained before, each bacteria species has a different behavior, their culture is fragile and can be easily contaminated. As the bacteria samples do not last more than five days in the culture and just some minutes under the microscope the experiments are hard to perform and require discipline.

2.2 Nanorobotics challenges

There are many challenges when it is considered the creation of a nanorobot. As explained by Akyildiz and Jornet, when it gets to the nanoscale, due to many physical restrictions, a new communication paradigm needs to be defined. According to the author vision, there are two main alternatives to network the *nanomachines*: nano-electromagnetic and molecular communications [Akyildiz and Jornet, 2010].

The first approach aims to transmit and receive electromagnetic radiation using new nanomaterials. On the other hand, the molecular communication envision to exchange information encoded in molecules, which already are in the nano scale. In another paper from the same author [Akyildiz et al., 2015], it is said that “the artificial nature of the devices could result in unwanted effects on health and pollution”, so the molecular communication approach using synthetic biology and nanotechnology tools becomes the best candidate inside the biological domain.

Akyildiz et al. explain that this kind of communication already exists in nature and it can be used to decode other kind of information, such as pollution level or other chemical concentrations. Some bacteria are capable to exchange specific DNA molecules between themselves and follow chemical trails to perform this exchange in distant ones. This is called *chemotaxis* and it is not the only process used by such microorganisms for orientation.

The magnetotatic bacteria possess another interesting behavior: the *magneto-taxis* which is the capability of being able to align and navigate along magnetic field lines. Therefore, this bacteria capability can be used in order to create a nanorobot. Many authors have developed projects using such behavior to control the magnetotatic bacteria using magnetic field and using it to push microstructures.

2.3 Magnetotatic Bacteria usages

One of the first studies to use the magnetotatic bacteria capabilities was performed by Bahaj et al. in 1998, where it was introduced a process to select specific magnetotatic bacteria in a sample [Bahaj et al., 1998]. As their dynamics are not deterministic, the main idea in the process is to select the ones with the desired behavior to enhance the culture. In this process, a magnetic field is applied over the sample so that only the susceptible bacteria swim across the channel. Then, these bacteria accumulate in the wall of the separator and when the capacity is reached they are separated from the rest of the sample. The culture would continue only on those susceptible bacteria. In this our project, this process of accumulating the bacteria in the wall is also used, but with the idea of generating a swarm.

Despite some other studies presented the micro manipulation of this bacteria [Lee et al., 2004a,b], only in 2006 that Martel et al. presented a paper showing the magnetotatic bacteria being used to manipulate other objects. The study demonstrate how to use *Magnetospirillum gryphiswaldense* bacteria to push $3\mu\text{m}$ microbeads along a predefined path. The experiments successfully showed that the bacteria could push

$3\mu m$ microbeads with a speed of $7.5\mu m/s$ and it proved the movement was being caused by the bacteria itself and not by the magnetic force drag [Martel et al., 2006].

One of the main challenges in this area is using the MTB to perform tasks in the micro scale. The Department of Computer and Software Engineering of the École Polytechnique de Montréal (EPM), directed by Prof. Sylvain Martel, carries many projects regarding the usage of magnetotactic bacteria as a *nanomachine*. In 2004, one of the papers showed the usage of Magnetic Resonance Imaging (MRI) to propel and guide magnetotactic bacteria inside the human body [Martel et al., 2004]. After that, in 2010, Martel and Mohammadi successfully demonstrated that the MTB could be used to perform micro-assembly tasks [Martel and Mohammadi, 2010]. Using a bacteria swarm of about 5000 bacteria, the scientists assembled a micro pyramid made of micro blocks. This proved the feasibility of using such micro organisms to perform tasks in the micro scale. It is interesting to point out that the MRI usage is more precise regarding tracking and magnetic field generation than the setup presented in our project, but on the other hand it is much more expensive. This group has developed many other researches about this topic and reached interesting results [Martel, 2006; Martel et al., 2004, 2009b; Martel and Mohammadi, 2010; Martel et al., 2009a].

Other applications of the bacteria are also being studied. Later in 2012, Ma et al. presented the full setup created to control another species of MTB, the *MO-1*, over a microfluidic chip, what introduces the usage of such microorganisms in the known “Lab-on-a-chip” device. The MTB are used to create microrobots, attaching $2\mu m$ Polystyrene (PS) microbeads to them. Those beads would make the visualization clearer and also open possibility to carry other chemical components. In the future, those microbeads could be used to perform chemical measures or detect diseases in patients blood, giving faster results. In our project, the setup is really similar to the one presented in their paper, which uses coils and a software to generate and control the magnetic field over the sample [Ma et al., 2012].

In both works described earlier the microrobot is constituted of a flagellated MTB with microbeads attached to it. Although this changes the movement dynamics of the bacteria, it is proven that using the proper techniques to attach the beads to the bacteria, they are capable of pushing them as a task [Martel, 2006; Ma et al., 2012].

In 2013 de Lima et al. presented a simple system and demonstrated the capability to control the *Magnetospirillum gryphiswaldense* position considering one axis only [de Lima et al., 2013]. Our work aims to continue this work using a different species.

Similarly to what was presented before, one of the objectives in this thesis is also to understand the behavior of a magnetotactic bacteria, in this case the species *Magnetofaba itaipuensis*. On the other hand, we do not aim to attach anything to the

bacteria as this technology is still under development in the NanoComp group.

The *Magnetofaba itaipuensis* was the first Southern Hemisphere isolated MTB and was presented by Morillo et al. in 2014. In his work, it is shown the isolation and cultivation of such species and its genomic analysis [Morillo et al., 2014]. Differently from the Northern cultivated MTB, this kind has a predominant South-seeking behavior. The culture of such microorganism is currently performed in the *Universidade Federal do Rio de Janeiro* (UFRJ) so it makes sense to use them in the experiments.

Differently from the previous projects, this work intends to address the problem related to the bacteria availability and the fact that the experiments are hard and expensive to perform. The idea is to realize experiments using a simulator instead of the real bacteria, making the process cheaper, faster and available to more people.

One of the first biological system to be modeled using computer was presented in 1966 by Levinthal. In this article it is presented an approach to simulate molecules geometric behaviors in order to understand their properties. Since then, many other researchers developed mathematical methods to model biological systems and with the increase of computational power more complex systems became candidate of such approach.

As said before, this simulation depends on the mathematical modeling of the system, in our case the magnetotactic bacteria. In one of the first studies of this kind of bacteria, Bahaj and James presents a method to extract a mathematical model from the MTB using image processing techniques. Using the images of the *U-turn* trajectory of the bacteria when the magnetic field is inverted, the magnetic dipole of the bacteria is obtained. The bacteria mathematical model is then extracted using the equations that govern the bacteria movement and the calculated dipole. The same process is also used by [Khalil et al., 2013] to obtain the mathematical equations that govern the bacteria. Some of the ideas presented in their work are used in our project, mainly the ones related to the innate characteristics of the bacteria (speed limit, inertia and responsiveness to the magnetic field). They have also shown that image processing can be used in such applications. On the other hand, the fact that the *Magnetofaba itaipuensis* has a different behavior and considering the setup limitations, some of the analysis cannot be performed the same way.

The validation of the simulator uses many techniques from Computer Vision. Considering the different mathematical models developed for replicating the bacteria behavior it is necessary to define some criteria to estimate the most similar one to the reality. On appendix B some basic concepts of Computer Vision are presented, followed by the presentation of the *Hough Transform* and the Optical Flow calculation, used in this thesis development.

Finally, though there are many articles showing the feasibility of the MTB control and showing advanced results on using the MTB to perform tasks, the current work uses a species never used before and aims to obtain the results using a low cost setup. Besides this, the MTB simulator would make the study of the applications of such micro organisms faster and accessible to groups without the bacteria or proper setup availability.

Knowing the state of art regarding the MTB usage, next chapter presents the methodology used in this thesis.

Chapter 3

Methodology

This chapter presents the setup for the experiments and how they were performed in this project. Besides this, the methods used to create the simulator are also shown.

This project has two different branches: the experimental and simulation phases. The main point is that they can be done separately and that the results of one can contribute to the other.

3.1 Physical Setup

This section focuses on the experiments performed using real bacteria. This part is focused on the setup and the methods created to do the experiments. The concepts used here goes from biology to optics and electronics.

3.2 Microscope

Using the equipment listed on appendix A it was developed the microscope setup presented in Figure 3.1. The distance between the Bi-Convex Lens and the camera is 15cm in order to match the lens focus. The mirror is used to reflect the image into the camera and the objective holder allows it to be exchanged. Both camera and sample holder are placed over stages that allow different position configurations and minor adjustments. Figure 3.2 shows a picture of the final setup with the important items highlighted.

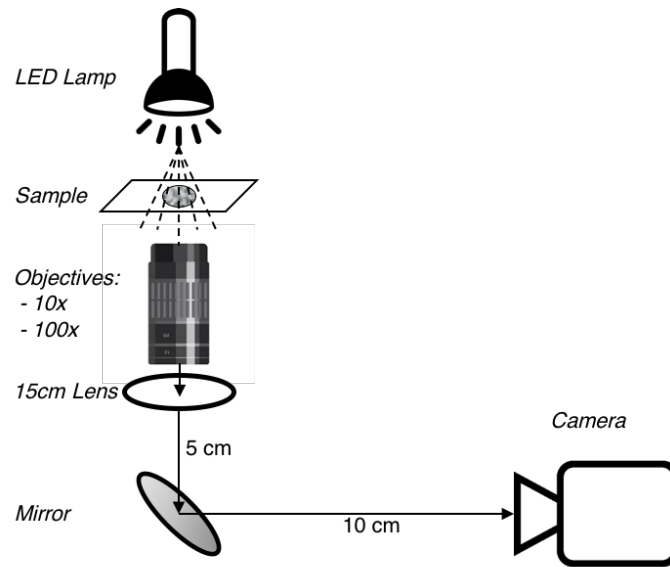


Figure 3.1. Experiment Setup. The setup allows changing the objective lenses and also moving the camera and the sample in order to change image position and small adjustments.

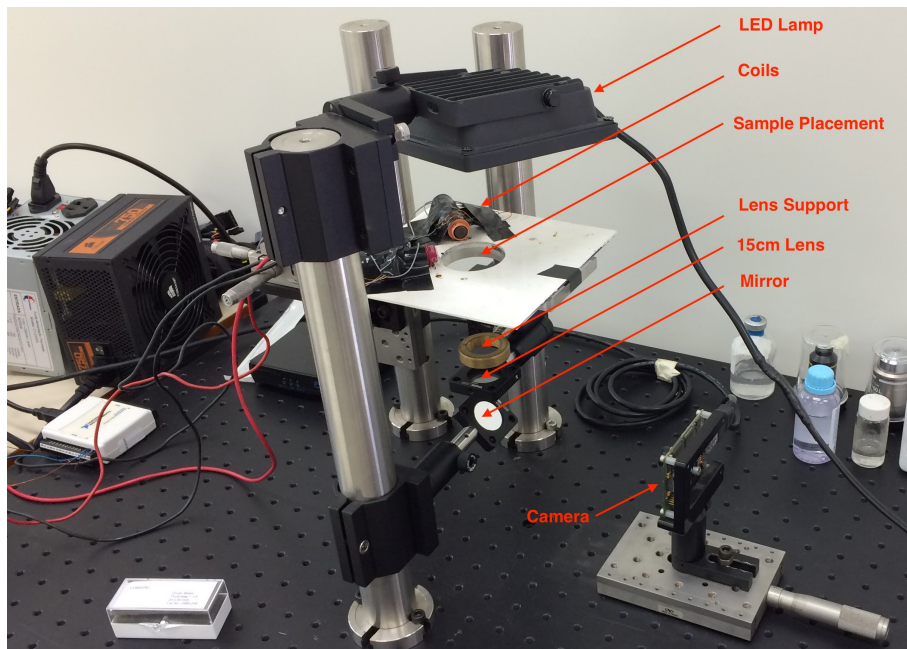


Figure 3.2. Picture of the final setup.

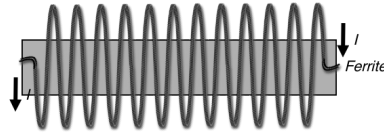


Figure 3.3. Coil that produces the magnetic field. The current in the wire can be inverted in order to invert the magnetic field direction.

3.2.1 Electronics

Two coils were used to generate the magnetic field around the bacteria sample. They were created curling a conductive wire around a magnetic ferrite, as it is possible to see in Figure 3.3. More information about the magnetic field generation can be obtained on appendix B.

Four of this coil are placed around the sample, as presented on Figure 3.4. This arrangement maximize the magnitude and allows different combinations of magnetic fields over the sample.

Two electronic setups were developed to change the magnetic field over the sample: manual or using a computer interface.

3.2.1.1 Manual Control

This approach uses a circuit with the schematic presented in Figure 3.5. In this setup, only two coils are used and both are driven by a $\pm 12V$ power source. Using the switch, the current direction in the coils are changed, consequently inverting the magnetic field over the sample. The switch $S1$ changes the power source, allowing the current inversion while the potentiometer $R3$ changes the resistance in the circuit affecting directly on the current magnitude. The diodes $D1$ and $D2$ blocks the short circuit on the different modes.

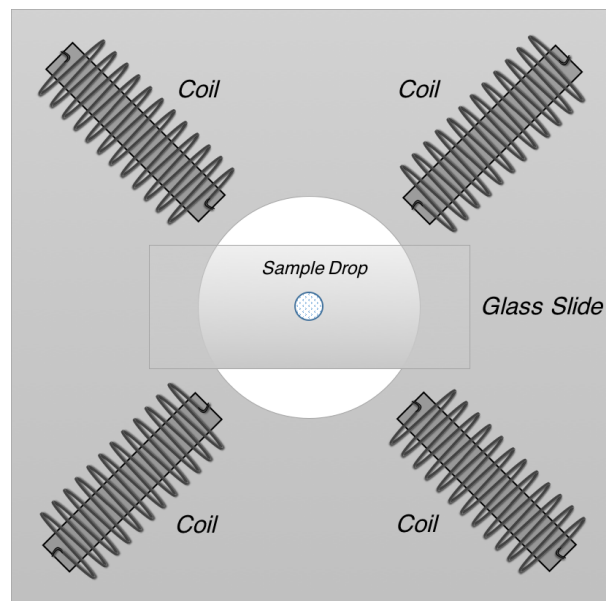


Figure 3.4. Top view of the board where the coils and the sample are placed together.

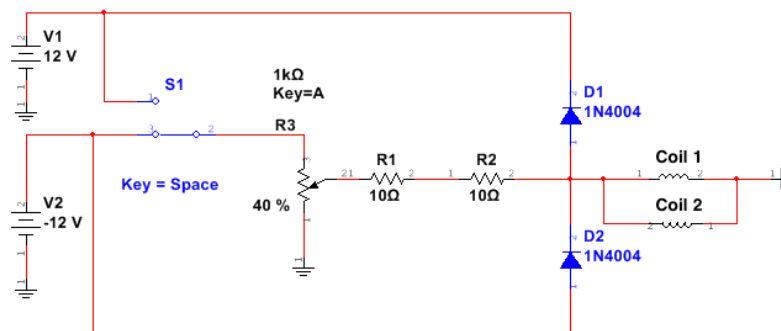


Figure 3.5. Schematic of the circuit to change the magnetic field direction manually. The switch $S1$ changes the power source and the potentiometer $R3$ changes the resistance in the system, thus affecting the magnetic field.

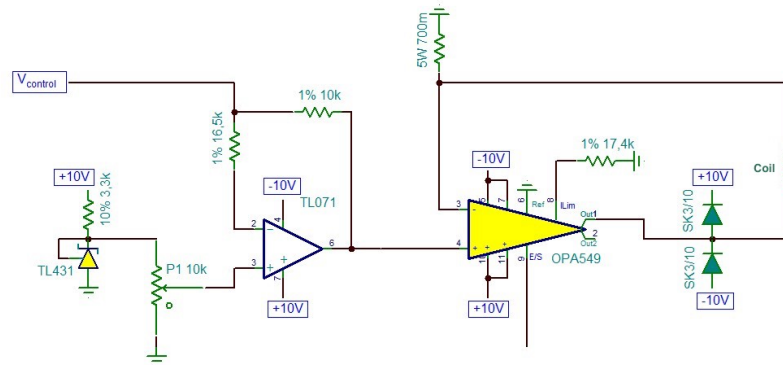


Figure 3.6. Amplifier circuit used together with the computer interface. It is responsible to amplify the value set by the computer.

3.2.1.2 Computer interface

On the second approach it is used the computer interface to act over the coils. The electronic system is responsible for amplifying the current applied to the coils based on a voltage input generated by the computer (Figure 3.6). Using the first amplifier, this voltage is compared to a reference value which is then used by another power amplifier to apply the correct voltage on the coil. The two diodes after the second amplifier are used to avoid big current changes on the coil when changing the $V_{control}$ value. Due to the heat dissipated by the power amplifier, this board is connected to a heat sink. Figure 3.7a shows the board and the heat sink. Four of this circuit were developed, one for each coil in the setup.

The $V_{control}$ voltage used in this circuit is provided by a National Instruments USB-6009 computer interface (Figure 3.7b) capable to generate a voltage between $0V$ and $5V$ on its outputs and also to read voltage values on its inputs. This interface is controlled using a program developed in *C*. This interface may be used by the controller to set the proper voltage on the coils.

For the experiments, the developed program has two operation modes: set the voltage to the maximum/minimum value or allow the user to incrementally change the voltage. The first mode is applied to observe the bacteria behavior to the magnetic field inversion and the second mode aims to observe how the bacteria responds to different magnetic field values.

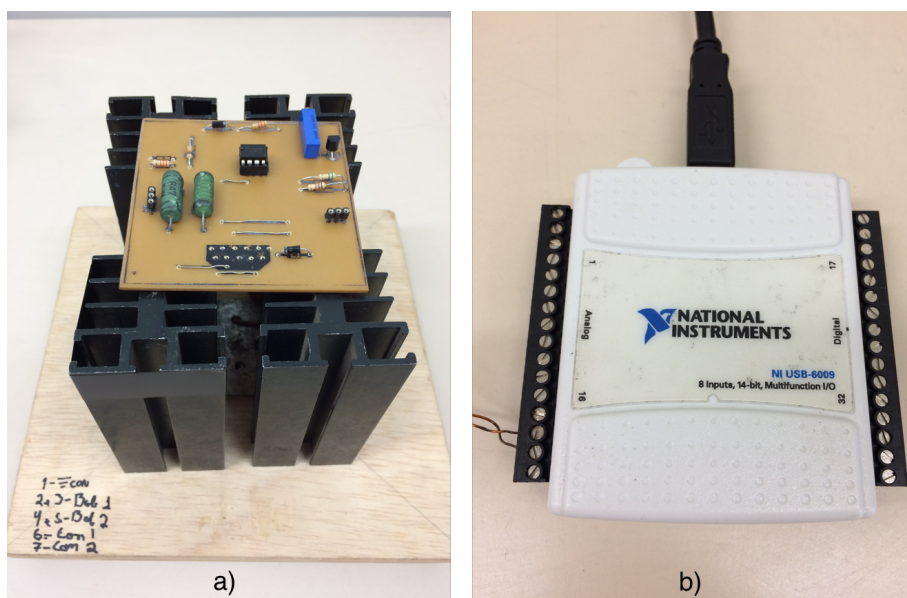


Figure 3.7. Electronic circuit (a) responsible for maximizing the current applied to the coils. Note the presence of the heat sink close to the Op Amps. The computer interface is done using the NI USB-6009 board (b).

3.2.2 Procedures

In order to avoid contamination of the sample and high exposure to Oxygen, the bacteria should be collected from the vessel using a sterilized syringe and put in a small Eppendorf Tube. From this tube, the bacteria drop is collected and placed under the microscope using a sterilized pipette.

As said before, the magnetotactic bacteria are microaerophile [Morillo et al., 2014] so the bacteria activity in the samples under the microscope does not last longer than ten minutes. This can be observed more in the edges of the drop, where the Oxygen concentration is higher. For this reason, the experiments must be fast and the samples must be changed frequently.

The microscope uses two possible objectives. Differently from the 10 objective, the 100 requires oil to work properly. This affects the experiments because a sample analyzed using the 100 cannot be reused with other objectives due to the oil present in the glass slide.

3.2.2.1 Image/Video Capture

As it can be seen in Figure 3.8, the camera preferences program allows to change the camera configuration, such as white balance, gain and frame rate.

Apart from this, other changes in illumination can be done looking for a better

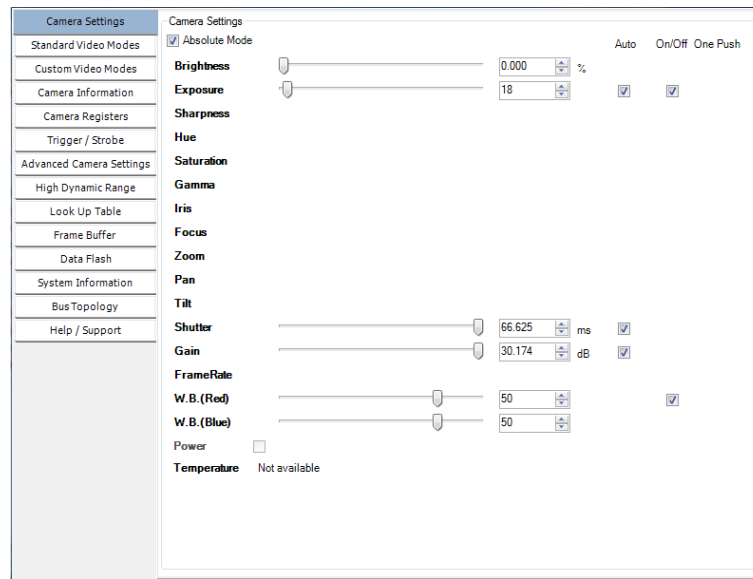


Figure 3.8. Dragonfly camera configuration. By default, the configuration are automatic but the user can change it manually.

image. The light direction can be changed in order to give an indirect illumination, for example. Besides this, the whole setup is covered in order to avoid noise coming from external lights.

The camera also allows to save images and videos. Figure 3.9 presents the record setup where it is possible to define the time of the videos, the number of frames and many other configurations.

3.3 Simulator

As said before, the experiments with the bacteria are difficult to perform due to a couple of reasons: the bacteria cultivation is difficult, the culture is really sensible to contamination and the bacteria die easily. For those reasons, it makes sense to model the bacteria behavior in the computer, allowing virtual experiments and the controller development and adjustments.

The simulator is developed using MatLab®. The reasons for choosing this tool is due to the facility to deal with data, many available toolboxes and easy GUI development.

The simulator architecture allows expansions and addition of new features and bacteria models. Figure 3.10 presents all available module and how they are organized.

Following a description of each model and the relationship between them.

Save Filename

Filename:

A timestamp, sequence number and file extension based on output type will be appended

Saving Options

Capture frames*

Capture 1 out of every frames from a run of frames*

Capture for ms

Capture once out of every ms from a run of ms*

* Specify zero to capture until manually stopped

Recording Mode

Buffered: Frames are buffered in physical memory while recording. Recording will stop if physical memory usage hits 95%

Streaming: Frames are not buffered in system memory while recording. Dropped frames may occur depending on the speed of the PC and the current camera/recording settings.

Only save corrupt frames when capturing

Images | Videos

Image Format:

PGM/PPM Options

Save as binary file

Good Frames: 0 Available Physical Memory: 0

Corrupt Frames: 0 Total Physical Memory: 0

Buffered Frames: 0 Usage: 0

Saved Frames: 0

Figure 3.9. Record configuration. Note that it is possible to define the file name, the size of the video and also the number of frames.

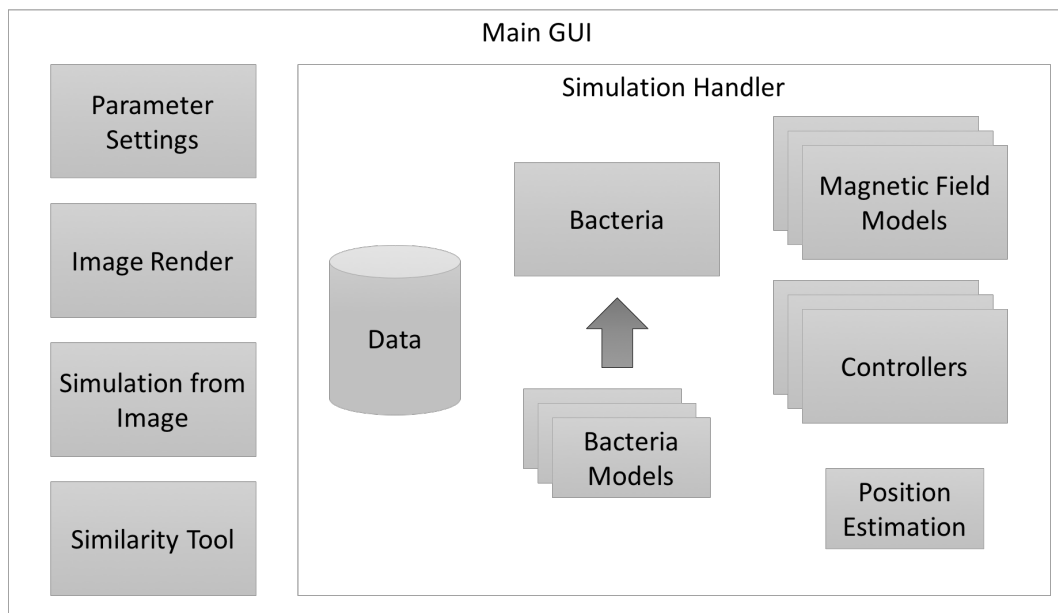


Figure 3.10. Simulator architecture where each block represents a module. The arrow represent the class inheritance between the Bacteria class and the different models.

3.3.1 Data

There are plenty of variables that are used by both the main GUI and the simulation handler. They perform the interface between the user’s configuration and how the simulation will behave. Apart from those setup variables, the simulation works basically over two data: the *grid* and the *bacteria* array.

The *grid* is a matrix that maps all available positions in the simulation and stores where each bacterium can be found. No bacterium can go over the grid limits and its size can be defined by the user or, if a real image is used as input, automatically identified by the simulator. If the real magnetic field modeling is used, the grid size is defined in order to match the simulation requirements.

The *bacteria* array stores objects of the “Bacteria class”, which represents the behavior of a single bacterium. At the beginning of the simulation, the user informs the amount of bacteria to be considered, what affects the size of the array.

3.3.2 Bacteria

The Bacteria class was developed in order to make it easier to implement new behaviors. Its objects represent each bacterium in the sample which are independent from each other. The base class “Bacteria” has the following properties and methods:

- Position (x, y) .
- Speed in each of the axis v_x and v_y . The signal indicated the direction of the speed vector.
- Bacteria size (pixels).
- *getPos()*: returns the current position of the bacterium $((x, y))$.
- *setPos(x,y)*: set the bacterium position to the informed values.
- *nextPos(grid)*: returns the next position of the bacterium using the internal speed. The *grid* information is used to avoid that two bacteria occupy the same position and to make sure that the new position is inside the *grid* limits.

The children class must implement the method *changeSpeed(maxSpeed, magX, magY)* that describes how the speed changes according to the magnetic field. Besides that, this class can add more properties and reimplement the object constructor to better model the bacterium behavior. In the simulation handler, this method is called every two iterations to simulate the inertia of the bacterium.

3.3.3 Bacteria Models

In order to model the bacteria behavior first it is important to define the basics on how to model a system. The bacteria models will be the base for the simulation and controller validation.

3.3.3.1 System Modeling

System Modeling is the area that studies different approaches to develop and implement mathematical models for real systems. When modeling a system, some assumptions are normally made regarding the model behavior. The model must be linear, it cannot vary in time and the variables change only with time, and not space. Besides this, a model may contain one or more variables and may also contain parameters that can be defined later in the modeling stage [Mendes, 2012].

There are basically two main approaches:

- White box modeling, based on the process physics;
- System identification based on observations.

The white box approach uses the physics knowledge to model the process behavior. For example, considering a wire where a current is applied. Using the Joule Law it is possible to preview the temperature of the wire when applying a specific current.

On the other hand, system identification is the procedure to obtain mathematical model capable of explaining the cause-effect relation between data in the process. Differently from the white box approach, some systems have many variables or are too complex to use known equation to extract a mathematical model for it. The idea in the system identification approach is to answer the following questions: is there any model that with the input $u(k)$ results in an output $y(k)$?

This procedure can be divided into the following steps [Mendes, 2012]:

1. Experiments and gather data;
2. Definition of the mathematic representation to be used;
3. Definition of the model structure;
4. Parameter definition;
5. Model validation.

In this work those concepts will be used to extract a mathematical model for the magnetotactic bacteria based on the experiments observations.

3.3.3.2 Basic Model

The first model was created based on the observations made during the first experiments. For each axis, it considers that the speed has two components: one random and one that depends proportionally on the magnetic field, according to Equation 3.1.

$$\rho_i = randi(2 * \rho_{max} + 1) - \rho_{max} - 1 + m \quad (3.1)$$

where ρ_i is the speed of the i^{th} bacteria, ρ_{max} is the maximum speed and m is the value of the magnetic field. This way, a speed will be generated between $-\rho_{max}$ and ρ_{max} and then the magnetic field m is considered. The MatLab method $randi(n)$ returns a value between 1 and n , so the subtraction is necessary to generate an output of $\pm\rho_{max}$. Based on this equation, the bacterium speed is proportional to the magnetic field magnitude and this way, when it is zero only the random component will be present. This equation is used to calculate the different speed magnitudes for each axis.

3.3.3.3 Adapted Model

According to the experiments performed previously, it was possible to see that the basic bacteria model behaves differently in some points. Considering this, a new model was created based on the mathematical model presented by Khalil et al. 2013.

In their work the force over the bacteria is described as a function of the magnetic force ($F(P)$) and torque ($T(P)$), where P is the bacterium position. This force is what is used to define how the bacterium will move. The author also mentions some other criteria that affect the bacterium movement, like the linear and angular velocity of the bacterium, the dynamic viscosity of the fluid, the size of the bacterium and also its rotation drag coefficient [Khalil et al., 2013].

Considering all information provided, a simplification was done and the adapted model presents the following behavior:

1. The magnetic field is only used for setting movement direction;
2. Each bacterium can respond differently to the magnetic field (including no response);
3. The bacterium has always the same innate velocity;
4. It has a small inertia.

In the first iteration, each bacterium is provided with velocity that can go from zero to the maximum speed defined by the user. After that, at every iteration the velocity in each axis is defined so that the resultant speed is the same as the previously defined. This is done using the magnetic field distribution in both axis. Besides this, the inertia is modeled considering a random value between $[-max_speed, max_speed]$.

In this new implementation, when the simulation starts it may be possible that some bacteria have zero velocity, meaning that they won't respond to the magnetic field. Even then, they still possess some random behavior as part of their movement.

Another important property considered in this model is the Earth magnetic field, which is being modeled in the Y axis with a value of one simulation unit. Considering this, if there is no artificial magnetic field applied in the sample, the bacteria tend to move up in the vertical direction.

3.3.4 Magnetic Field Models

The simulator considers two approaches to model the magnetic field over the sample. The first one considers that the magnetic field vector is the same in the whole sample.

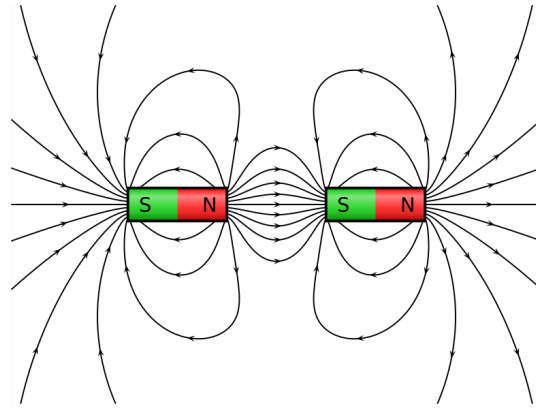


Figure 3.11. Magnetic field when both coils generate the magnetic field lines in the same direction [Wikimedia Commons, 2016].

On the other hand, the second approach is based on the *Biot-Savart* description of the magnetic field.

3.3.4.1 Constant Magnetic Field Model

This basic implementation considers that the magnetic field vector affects all bacteria in the sample in the same way. Meaning that the field applied in a bacterium in the edge is the same as the one applied in any another point of the sample.

Considering the setup presented in Figure 3.4, this model has two representations in the experiments: only one coil being used or both coils in the diagonal with the same magnetic field direction. The difference between them is the observed magnetic field magnitude in the sample, which is expected to be higher when using two coils.

3.3.4.2 Biot-Savart Model

Another approach to model the magnetic field is using the *Biot-Savart* law (more information available on appendix B. As it is possible to see in Equation B.6, the distance from the coil changes the magnitude of the magnetic field observed in each point. Using two coils results on creating a region with null magnetic field around the sample.

Consider a situation where the current in the coils generates a magnetic field on the same direction, as seen in Figure 3.11. In this case, the vector in the sample has the same direction of the magnetic field created by the coils.

On the other hand, if the coils produce magnetic field with opposite directions (Figure 3.12), there is a region between the coils where the magnitude of the magnetic field is zero. This region with zero gradient is interesting because, if it is considered

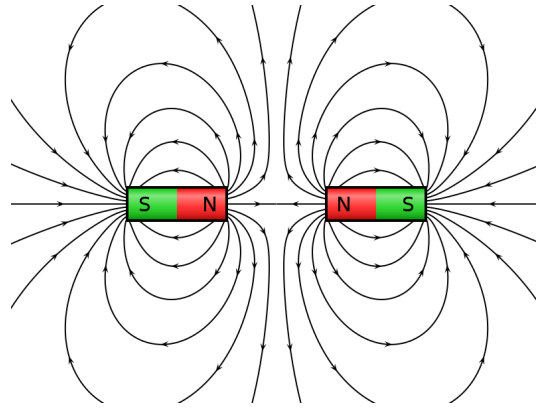


Figure 3.12. Magnetic field lines when the coils generate magnetic fields in opposite directions. Between the coils the magnitude of the magnetic field is zero [Wikimedia Commons, 2016].

that the bacterium aligns based on the magnetic field, this region would automatically agglomerate the bacteria. This is why this second approach is promising, as it is possible to control the swarm position simply setting the gradient to the desired position.

For practical purposes, it is considered the solenoid as ideal, where the turns are closely spaced and the length is greater than the radius of the turns. To find the magnetic field on a limited plane with desirable time, the radial field of the solenoid is calculated as proposed by Callaghan and Maslen and then the axial field of the solenoid as proposed by Derby and Olbert. The magnetic field calculations are done with the help of the scripts developed by Cebon [Callaghan and Maslen, 1960; Derby and Olbert, 2010; Cebon, 2015].

With the magnetic field information and the bacterium position, it is possible to calculate what is being applied on each bacterium. The Figure 3.13 shows a visual representation of the matrix generated by the simulator. The magnetic field matrix is also used to define the grid size in the simulation.

The problem with this approach is that the calculations have a relatively high computational cost compared to the simulation itself. Thus, it is not possible to perform it at each iteration, making necessary to create a way to use such information in real time without affecting the system performance.

The solution is to calculate multiples magnetic fields for multiple combinations of relevant currents and store the results in a file. This file contains the gradient position and the magnetic field matrix together with the correspondent currents that should be applied to the coils.

In the simulator, this file is loaded so all the pre-computed values are available. This way, the control is done simply looking in the table for the closest gradient to the

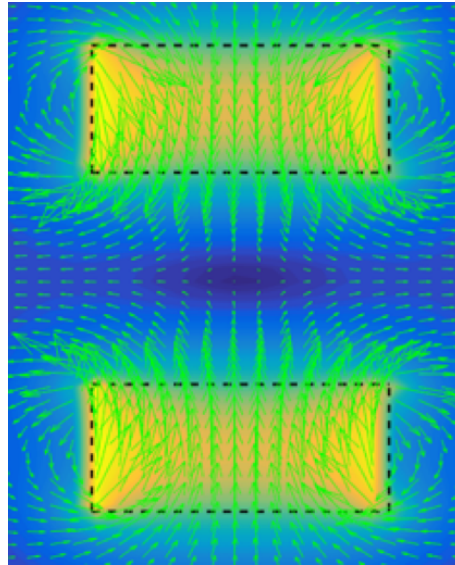


Figure 3.13. Magnetic field lines generated by the script [Cebon, 2015]. This matrix has a gradient and is generated by a certain combination of currents in each coil.

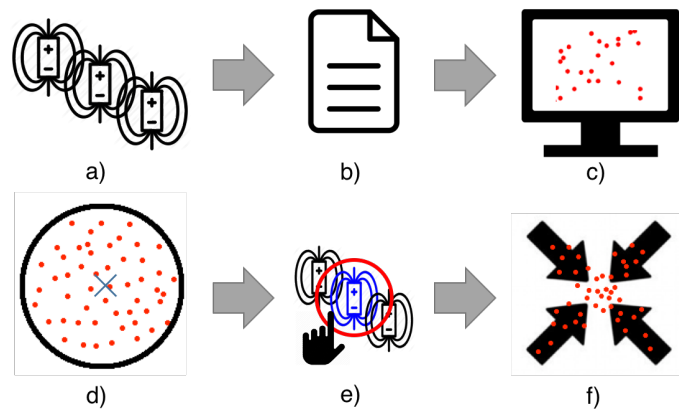


Figure 3.14. Process to use the real magnetic field data on the simulator. (a) the magnetic field matrix is calculated for many combinations of currents in each coil, (b) data is stored in a file, (c) the file is loaded in the simulator, (d) during the simulation the setpoint is informed, (e) find a matrix that the gradient is the closest to the setpoint and (f) apply this matrix to the bacteria set.

setpoint position and then, using the correspondent magnetic field matrix to recalculate the bacteria position. The full process is shown in Figure 3.14.

3.3.5 Controllers

This session presents the controllers of the magnetic field that allows handling the bacteria. There are two main approaches to control a system: open and close loop

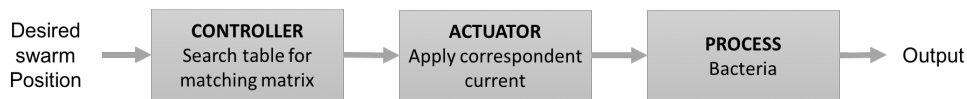


Figure 3.15. The magnetic field approach where it is possible to create a magnetic field gradient over the sample. This approach consists on an open loop control of the swarm position.

control [Dorf and Bishop, 1998].

3.3.5.1 Open Loop - Magnetic Field Gradient

The Open loop control acts over the system without considering its output directly (no feedback). It considers that there are specific combinations of actions that will make the interested variable reach an specific value.

The flow presented on Figure 3.15 shows how the Magnetic Field Gradient is used to control the swarm position. The controller is represented by the magnetic field simulation database, the actuator is the current applied to the coils in order to obtain the gradient in the desired position and the process is the bacterium acting according to the magnetic field gradient. There is no feedback in the flow, so there is no usage of the swarm position in the control.

3.3.5.2 Closed Loop - Fuzzy Controller

Considering the scale of the experiments, creating a precise magnetic field gradient over the sample is a big challenge. The control over the current in the coils is limited and the experiment setup affect how the magnetic field. Therefore, for simplistic reasons, the magnetic field over the sample may be considered constant.

Assuming this, the other approach to control the swarm is to use a feedback control flow as seen in Figure 3.16. Differently from the open loop control, the current position of the swarm is considered by the controller to decide what should be the action over the actuator. So, besides the controller itself, it is necessary to develop a strategy to measure the average swarm position.

Fuzzy control provides a method for constructing nonlinear controllers using heuristic information, which makes it a practical alternative for challenging control applications. That heuristic information may come from an operator that acts as a "human-in-the-loop" controller, who is asked to define a set of rules on how to control the process. It may also come from a control engineer who has performed extensive mathematical modeling, analysis and development of control algorithms for a particular process. In the fuzzy control design methodology, those rules are incorporated into

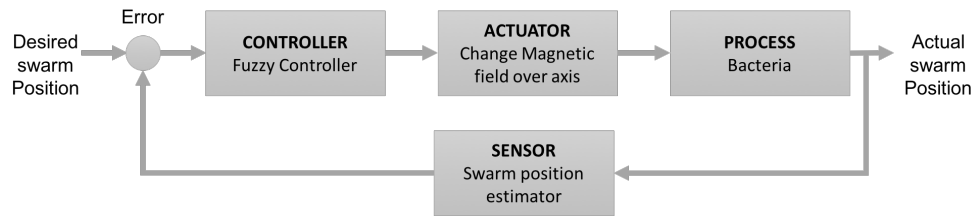


Figure 3.16. Closed loop approach using a Fuzzy controller. Instead of changing the current, this controller act directly over the magnetic field of the system. The process is the same but this approach requires a swarm position estimation to be used in the controller.

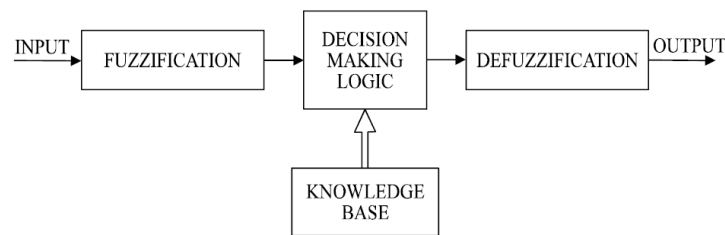


Figure 3.17. Block diagram of a fuzzy controller [Simoes, 2010].

a fuzzy controller that emulates the decision making process of a human [Moore et al., 2009].

As shown in Figure 3.17, a fuzzy logic system has four blocks. The fuzzification block converts crisp input information into fuzzy values for each input fuzzy set. Fuzzification is the process of decomposing a system input and/or output into one or more fuzzy sets, allowing system inputs and outputs to be expressed in linguistic terms so that rules can be applied in a simple manner to express a complex system. Rules are logical implications, expressed as *If <condition> Then <consequence>*, that associate conclusions with conditions.

The decision-making-logic determines how the fuzzy logic operations are performed and, together with the knowledge base, determine the outputs of each fuzzy rule. After that, the linguistic output variable needs to be translated into a crisp value. The objective is to derive a single crisp numeric value that best represents the inferred fuzzy values of the linguistic output variable. The process of mapping the output from the fuzzy domain back to the crisp domain is executed by the defuzzification block [Simoes, 2010].

In this project the Fuzzy approach is recommended because there is no exact model of the bacteria swarm. Besides this, they can be easily upgraded simply adding more rules to the system.

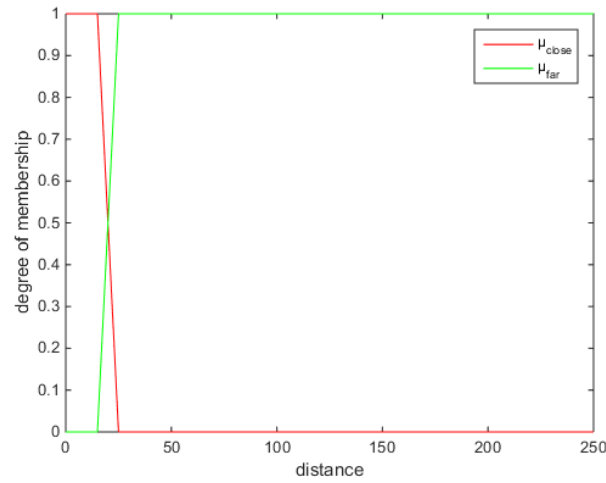


Figure 3.18. Membership functions used in the IF-THEN rules. The red function represented the concept for "close" while the green represents "far".

The fuzzy control is based on rules to emulate the "human-in-the-loop". For the project of this controller it is considered the distance between the swarm and the defined setpoint. For that, two really simple IF-THEN rules are created:

IF swarm is close THEN magnet field is half.

IF swarm is far THEN magnetic field is maximum.

The membership functions for "close" and "far" are $\mu_{close}(d)$ and $\mu_{far}(d)$, respectively. Both membership functions were defined as trapezoidal, as shown in Figure 3.18.

The inference is made using Sugeno inference mechanism [Sugeno, 1985], as shown in Equation 3.2, and the graphical representation of the result is shown in Figure 3.19. This way, the controller is represented by the result of this equation together with the value of d , obtained by the position estimation.

$$M_s = \frac{\mu_{close}(d) \cdot M_{close} + \mu_{far}(d) \cdot M_{far}}{\mu_{close}(d) + \mu_{far}(d)} \quad (3.2)$$

where $M_{close} = m_{max}/2$, $M_{far} = m_{max}$ and m_{max} is the maximum value of the magnetic field.

3.3.5.3 Position Estimation

The closed loop approach uses the current estimated position of the bacteria swarm to control the system. Depending on the application, there are some options that can be considered to obtain this information.

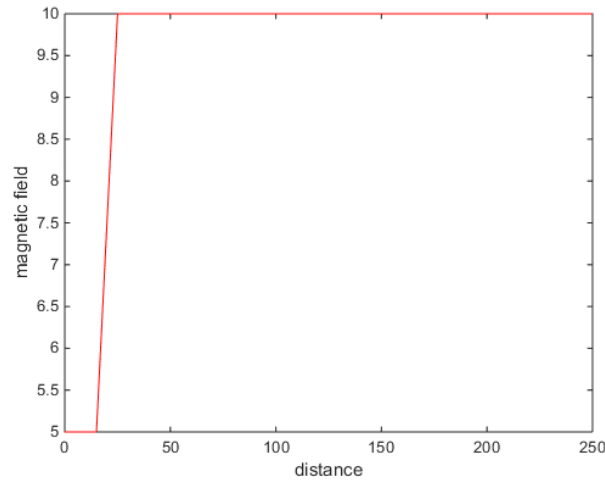


Figure 3.19. Result of the inference process. It shows the relationship between the distance between the bacteria swarm and the setpoint and the magnetic field to be applied over the sample.

In the simulator, as the position of each bacterium is known and it is expected to see only one swarm in the sample, the calculation of the bacteria swarm is performed using the average position of all bacteria.

This is a very simple approach, as it does not consider the bacteria dispersion in the calculation and also restrict the simulation to a single swarm. To enhance this model it may be consider some fuzzy logic to help to define what is considered a swarm and identify multiple groups.

3.3.6 Simulation Setup

The main GUI presented in Figure 3.20 allows the user to configure how the simulation will be performed. The following parameters can be configured using this interface:

- Bacteria model.
- Controller model.
- Number of bacteria in the simulation and their maximum speed.
- Setpoint configuration.
- Record options.
- Magnetic field model.

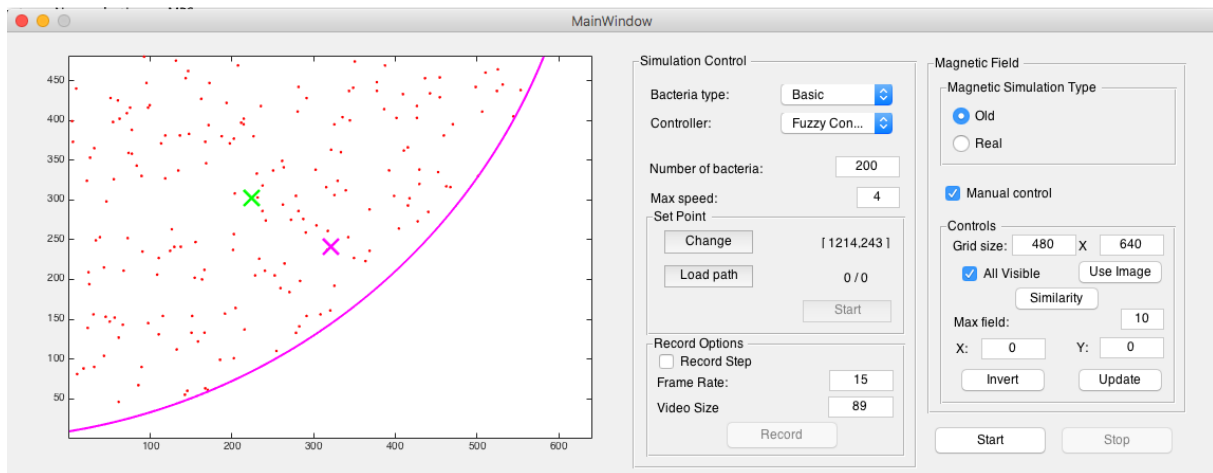


Figure 3.20. Main GUI of the simulator. It allows changing the parameters used in the simulation.

- Magnetic field manual control.

In the simulator, the image is represented by a graph which size correspond to the *grid* or to the experiment image used to setup the simulation. The image in the graph represents the image seen in the experiments. Each bacterium has its own position in the grid and it is represented by a dot in the image. At each iteration the graph is replotted, updating the bacteria positions.

There are two configurations that affect how the simulation will behave according to the presented image.

3.3.6.1 Constrained Simulation

In this case, the simulation is constrained by the limits of the grid, whose size is defined by the user. All existent bacteria in the simulation are visible and there is no obstacle inside the grid. As it seen in Figure 3.21, the bacteria cannot trespass the grid limits. The green cross represents the average position of the bacteria swarm while the purple one the initial setpoint used by the controller.

3.3.6.2 Simulation from Experiment

The constrained simulation is interesting to test the models and to visually verify their behaviors, but when one needs to compare the models accuracy it becomes necessary to use the real experiments images.

In all performed experiments, saved images correspond to one of the borders of the drop. So, in order to have the same restrictions on the simulation as is seen in

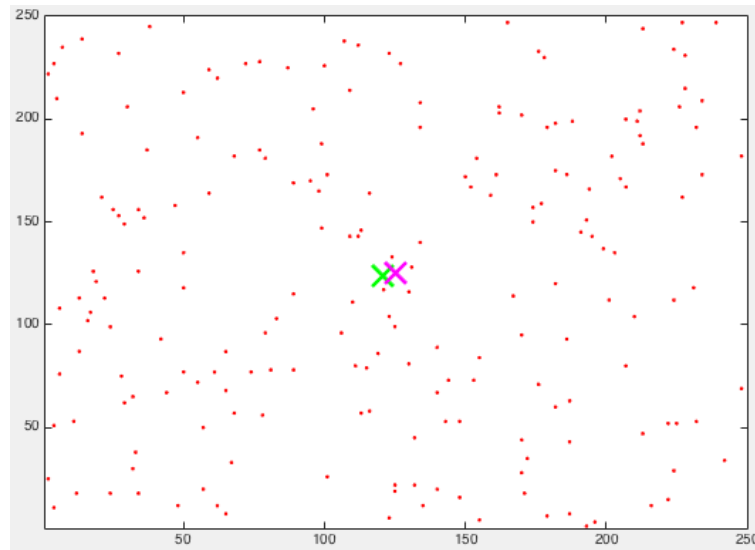


Figure 3.21. Simulation constrained by the grid limits defined by the user. In this case all bacteria existent in the simulation are visible to the user.

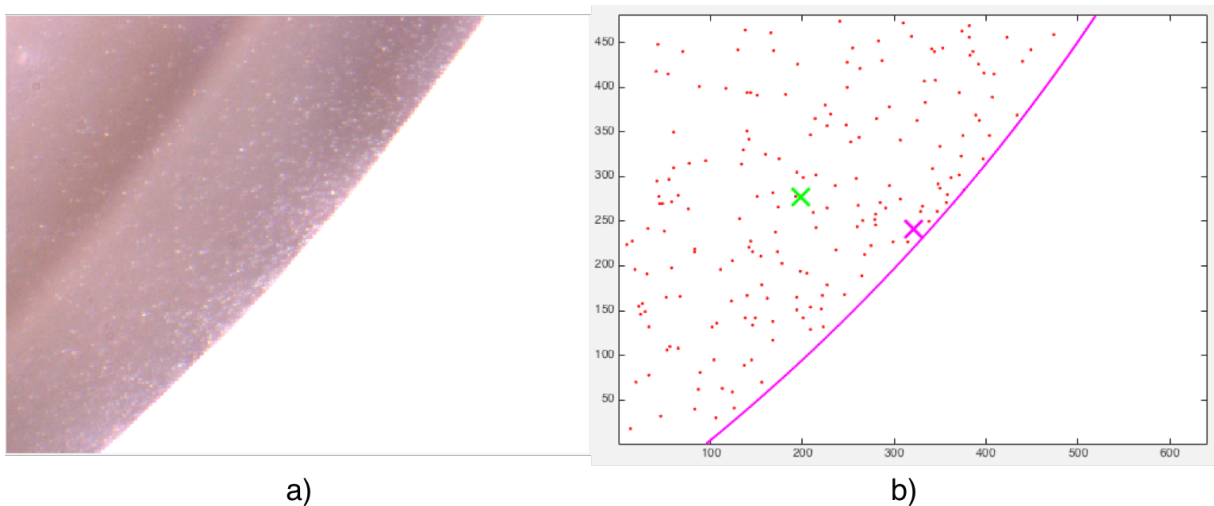


Figure 3.22. Figure (a) shows a image from a experiment and (b) the simulation using the same constraints

the reality, two restrictions must be observed: the bacteria cannot trespass the drop border and the bacteria can move outside the field of view and return, depending on the magnetic field. Figure 3.22a shows the image obtained during an experiment where the bacteria swarm is accumulated in the drop border. On the other hand, Figure 3.22b shows the simulation running with the same constrains as the experiment.

To extract the initial state setup, computer vision techniques are applied considering some assumptions regarding the experiments. First, it is necessary to assume that the drop is a full circumference and the border seen in the image is part of it.

Then, the following methodology is defined to identify the border limits and grid size:

1. Read video from experiment and get the first frame.
2. Transform image into gray scale and smooth it using Gaussian filter.
3. Find image edges (Robert's algorithm [Lawrence, 1963]).
4. Use the *Hough Transform* to identify the lines in the image.
5. Using the lines extremities, find the circumference that fits best those points.

Figure 3.23 shows the whole process to extract the simulation setup from the image. In this process, the *grid* size is defined by the radius of the identified circumference and the axis size is defined by the image size, in pixels. Note that the grid size is bigger than the axis, so not all bacteria in the simulation is visible at all times. To make the experiments faster, before starting the simulation, it is possible to choose an option to place all bacteria initially exclusively in the visible area.

3.4 Analysis Tools

The simulator quality and performance can only be evaluated if it represents what is seen in the experiments. Thus, it becomes necessary to develop some tools to analyze the results obtained and evaluate the current implementation.

For this, two tools are proposed: activity evaluation and difference estimation. First it is important to define the procedure used to capture the videos.

3.4.1 Bacteria Step Response

The step response of a system can be used to obtain its mathematical model regarding time. The procedure consists in giving a step input to the system and observe its output. On the current system, the step input consists on inverting the voltage applied to the coils, what causes the inversion of the magnetic field direction (Figure 3.24).

To capture the bacteria response to the step, the following procedure must be followed:

1. Accumulate the bacteria in one of its borders.
2. Find in the sample the position where they are accumulating.
3. Invert the magnetic field direction (invert voltage on coils), capturing the images.

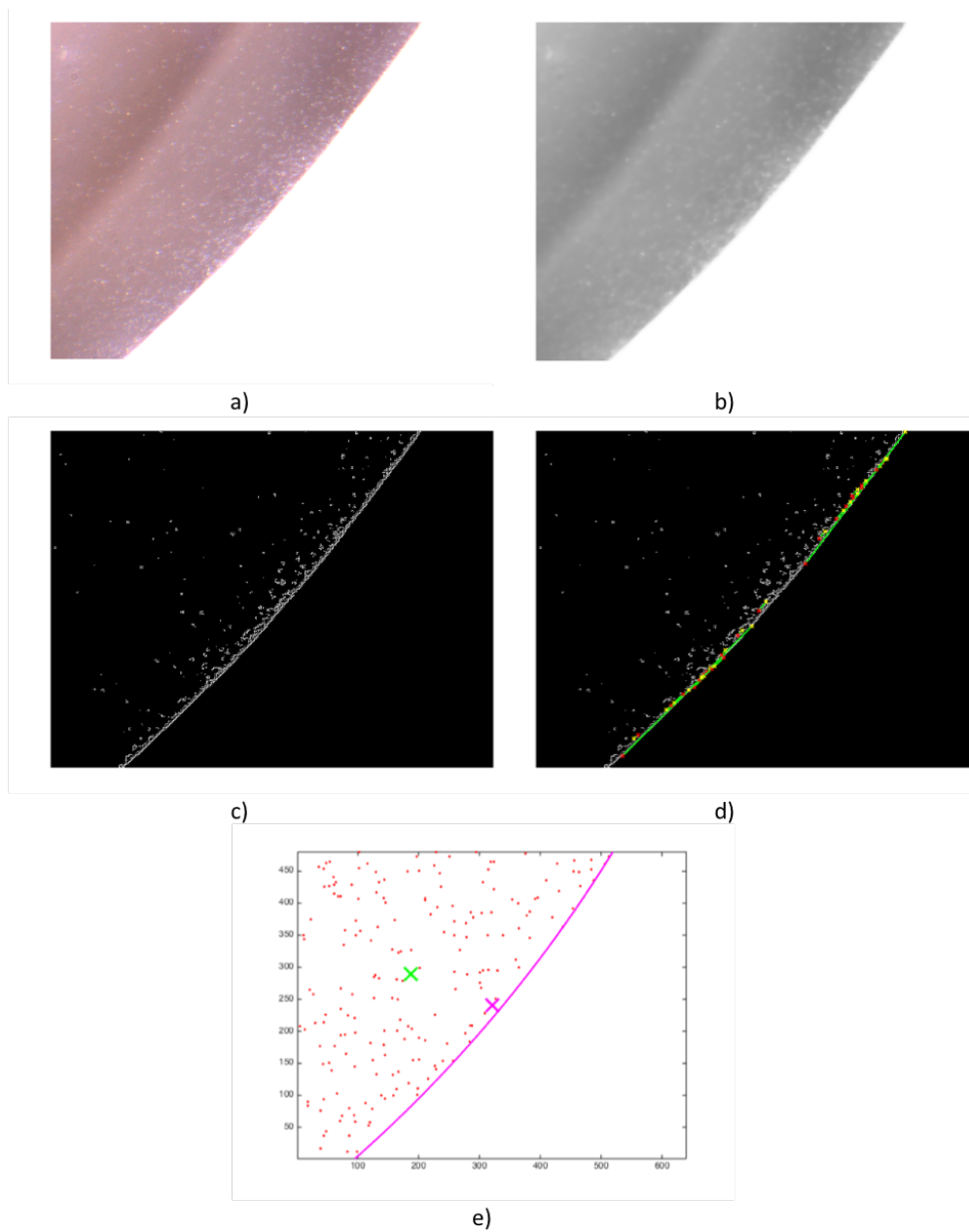


Figure 3.23. (a) First image from a video obtained on an experiment, (b) image in gray scale after filtering, (c) detected edges in the image, (d) lines identifies using *Hough Transform* (red and yellow dots representing the extremities of the lines) and (e) simulation using the image setup.

In the Figure 3.25 it is possible to see the behavior of the bacteria when the magnetic field is inverted. In Figure 3.25a the magnetic field accumulate the bacteria in the border. After inverting it, the bacteria start moving in the opposite direction, as seen in Figure 3.25b and 3.25c. The bacteria step response video corresponds to

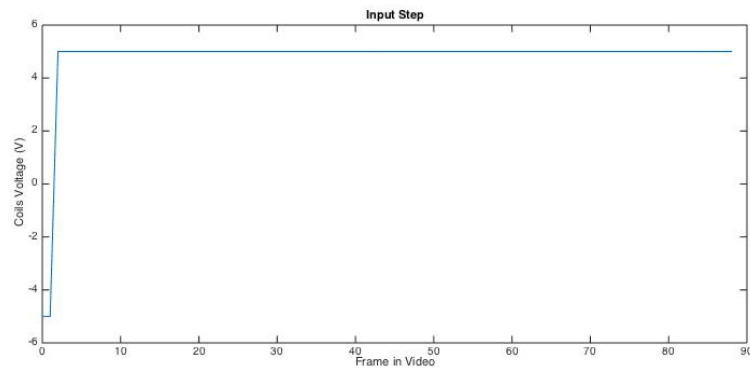


Figure 3.24. Step input applied to the coils.

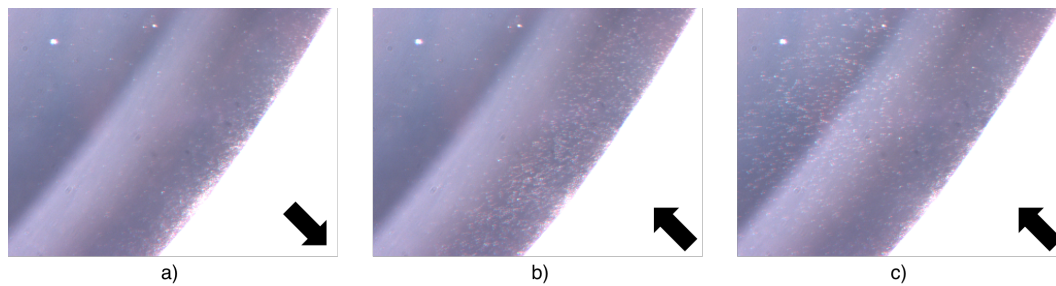


Figure 3.25. Step response of the bacteria. On (a) the magnetic field direction makes the bacteria to accumulate in the border. After changing its direction, the bacteria moves in the opposite direction as seen in (b) and (c).

the video starting right after the voltage is inverted and lasts for six seconds (about 90 frames).

The same bacteria response is obtained using the Simulator. For that, using the same initial setup of an experiment, it is possible to simulate the step response of the simulated bacteria and save the correspondent video. For the difference estimation purposes, the Optical Flow of the video is also calculated during the simulation and stored in a separate file.

3.4.2 Activity Evaluation

Considering that the bacteria are microaerophile, it becomes interesting to analyze its activity during the time when it is exposed to Oxygen. In order to do so, it is proposed a method to estimate and compare the bacteria activity throughout the experiment. For about 15 minutes, videos of the bacteria step response were captured using the same setup, as shown in Figure 3.26. It is important that the same procedures are performed in all videos avoiding brightness variations and position changes.

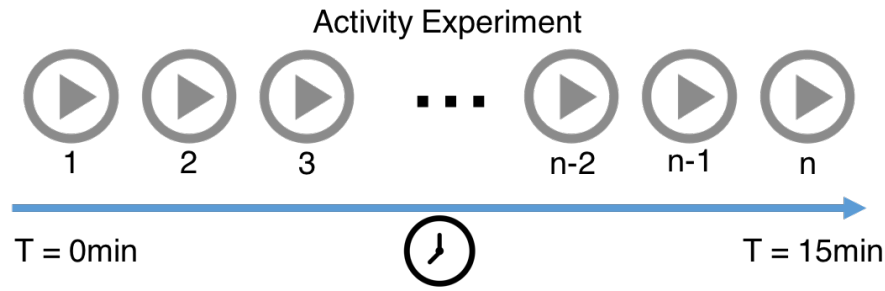


Figure 3.26. Method created to capture videos and evaluate the bacteria activity. The same setup is used to capture multiple videos in different times.

Using the *Horn-Schunck* algorithm, the Optical Flow between two frames are calculated. Considering that on the step response videos, all bacteria that respond to the magnetic field change will move on the same direction, the matrices returned by the algorithm are filtered, removing noise and not relevant data. Figure 3.27 presents the optical flow before and after being filtered.

Finally, both matrices are summed up, resulting in a number that represents the instantaneous activity in the video on that frame. Then activity is calculated for all frames resulting in an activity signature. This information is used to compare the videos and to observe the activity changes through the time.

3.4.3 Difference Estimation

In order to avoid using the visual perception criteria to define a “good” or “bad” model, it is presented a process to evaluate the difference between the bacteria behavior observed during the experiments and the one seen in the simulation. This way, it should be possible to identify the most similar bacteria model and its parameters to implement and test the controller using only the simulator.

The estimation has some assumptions: the video from the experiment cannot vary the edge position neither the image brightness and the video from the simulator must have the same initial state as the experiment (same drop edge location). In both videos it is also expected to see the bacteria being stimulated the same way, in this case with the step response.

The process involves processing the videos and comparing the bacteria activity using Optical Flow. Then this information is used to estimate the difference between each combination of frame. The difference is defined so that closest it is to zero, the more similar the two videos are in that specific time. Figure 3.28 presents the Optical Flow of the experiment and simulation video. Note the concentration of vectors on the

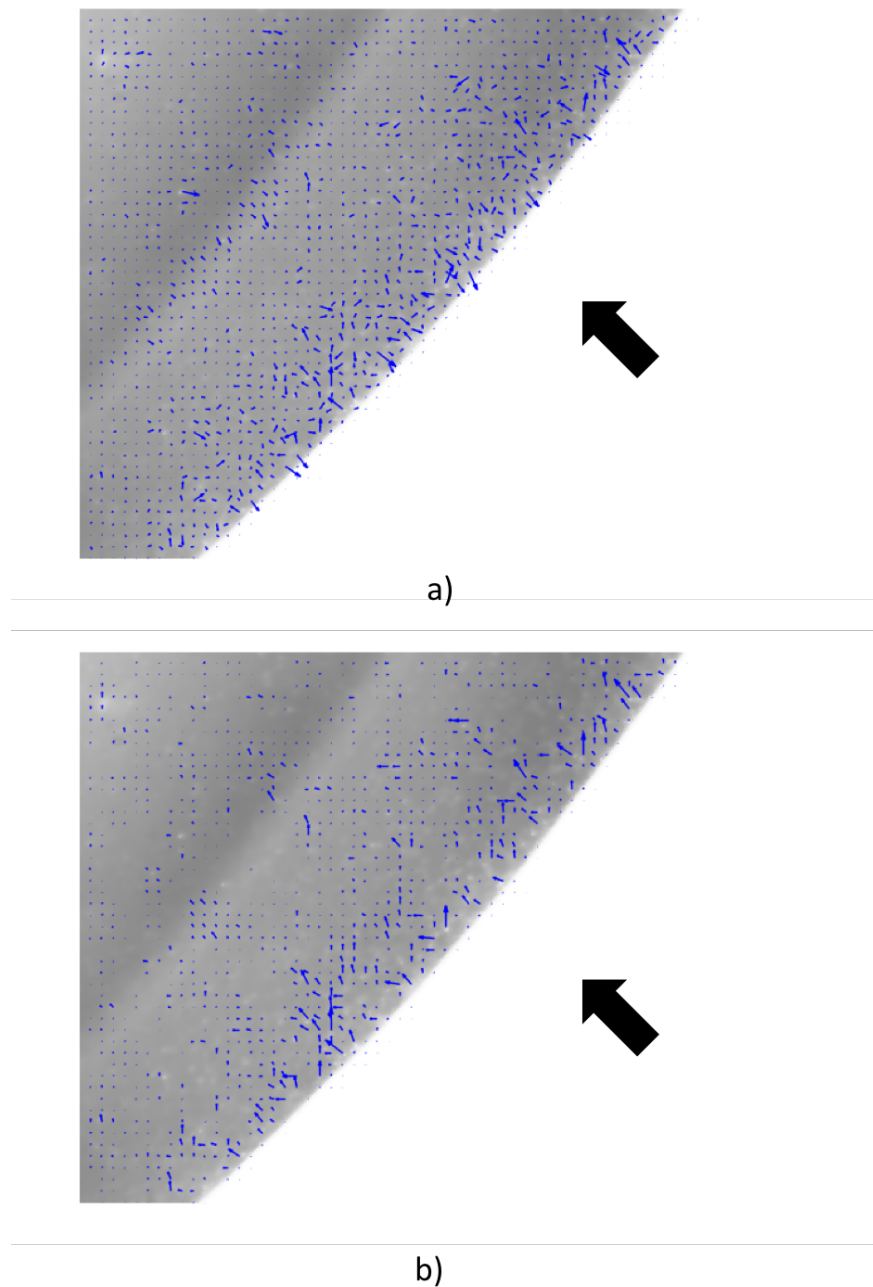


Figure 3.27. Optical flow calculated on the image (a) and after the filtering (b).

swarm position (next to the edge).

To reduce noise in the analysis, the Optical Flow of the simulation videos is extracted together with the video generation and it is stored as a separate file to be used in the difference estimation analysis.

The process is as follows:

1. Open videos and while they are not finished:

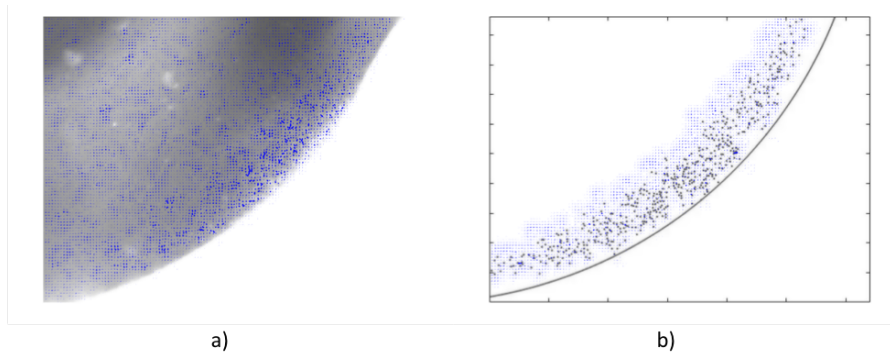


Figure 3.28. The blue vectors represent the Optical Flow in the experiment (a) and simulation video (b).

- a) Capture two consequent frames from each video and process the images;
 - i. Calculate the Optical Flow between two consequent frames in the experiment video using *Horn-Schunck* method;
 - ii. Obtain the Optical Flow of the simulation video from the stored file;
- b) Process both Optical Flow, filtering out movements not in the expected direction;
- c) Using Quadratic-Chi Distance, calculate the difference between both Optical Flows, which represents the instantaneous difference between the experiment and simulation videos at this given frame;
- d) Store the difference calculation through the videos.

2. Data analysis to define the overall difference between the videos.

As said before, the comparison is performed using Optical Flow. The *Horn-Schunck* algorithm returns two matrices with the flow value in each axis (u is the vector projection in X and v the projection on Y axis). Together, these matrices show the magnitude and direction of the flow in each point of the image. To process this matrices and get a single array they are filtered, keeping only the desired movement. Then, each column of the u matrix is summed up resulting in a vector that represents the overall activity in the X direction (du/dx) and each row of the v matrix is also summed up, representing the activity in the Y direction (dv/dy). For the sake of simplification the dimensions du/dy and dv/dx are not considered for the difference estimation. This generates two histograms that represents the interested movement in each direction. Figure 3.29 presents the calculation being performed between two frames of a video

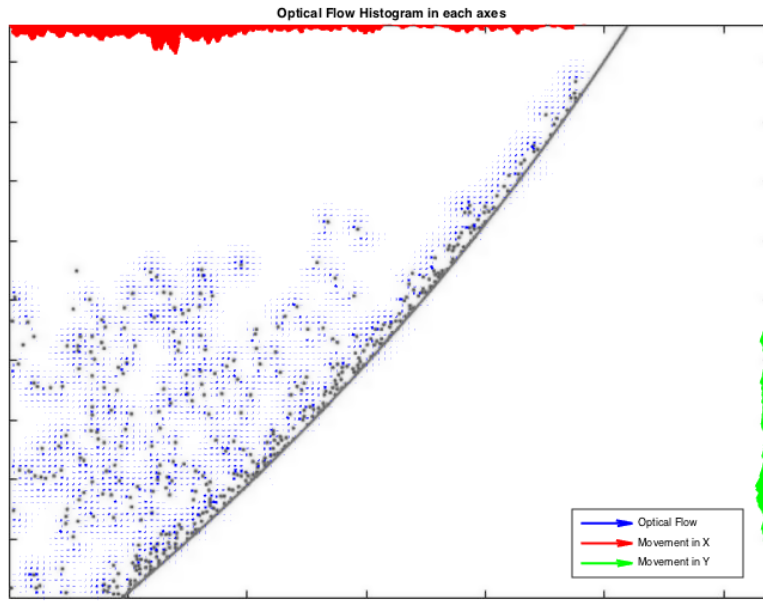


Figure 3.29. Flow Histogram on the image split into each axes. The red shows the movement in the X and the green in the Y . The blue arrows are the filtered optical flow.

generated using the simulator. The red histogram shows the movement in the X while the green shows the movement in Y .

These two histograms obtained on both videos are compared with each other using Quadratic-Chi Distance, that measures the difference between them (zero is the difference measured when a histogram is compared to itself). This value represents the difference between the two videos at this frame. More information about this method can be obtained on appendix B. The difference is calculate till the end of the videos resulting on a array of differences.

3.4.4 Data Analysis

The simulator validation consists in identifying the best bacteria model and its parameters in order to achieve a simulation as close as possible to the behavior seen in real experiments.

As shown in Figure 3.30, in this methodology, for each experiment a single real video is used as reference and, based on its initial state, some simulations are performed with different bacteria models and parameters. Then, the simulation videos are compared to the reference in order to evaluate the differences between them.

Considering each model, it is defined five different parameter configurations and

three videos are generated for each one using the bacteria step response. So, for each experiment the analysis will be done using 15 simulation videos.

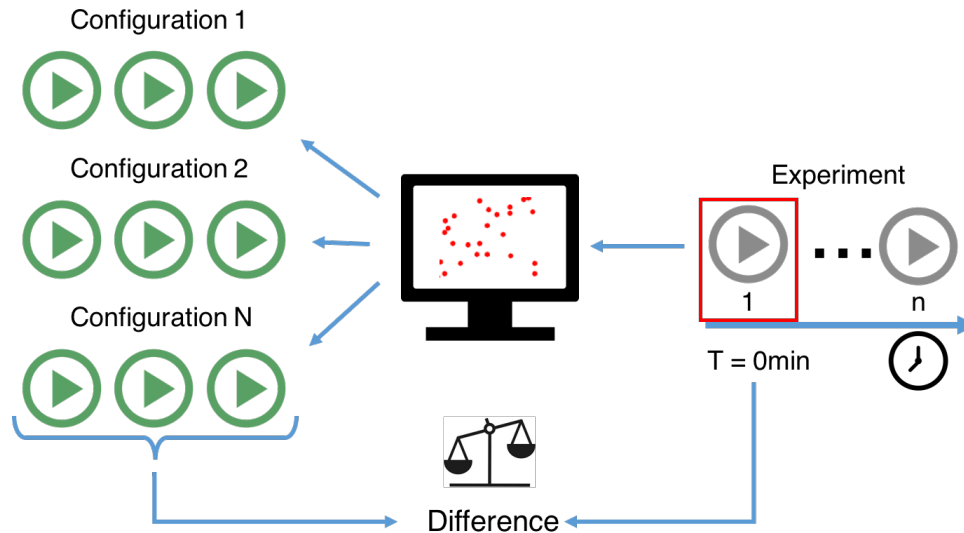


Figure 3.30. The first frame of the reference video is used to setup the initial state for the simulation, which is run with different models and different parameters. Then, each simulation video is compared to the reference to evaluate their difference calculation. For five difference configurations it is performed three different simulations.

3.4.4.1 Best Model Identification

To identify which bacteria model produces simulations more similar to the real experiments it is used the overall average difference. This is obtained considering the average difference from all simulations performed for a specific bacteria model.

3.4.4.2 Best Parameter Identification

For each bacteria mathematical model it is necessary to identify which parameter gives simulations more similar to the real experiments. In both developed models the only flexible parameter is the bacteria maximum speed.

This analysis is done using a linear regression on the instantaneous differences calculated throughout each simulation.

Considering the line equation $y = ax + b$, where a is the line slope and b is the point where the line cuts the Y axis, the smallest the slope of the curve, the more similar the simulation video is to the reference experiment. The baseline for this calculation is the fact that, when comparing an experiment video to itself, the result

is a line with a and b equal to 0. This would correspond to an ideal scenario where the simulation produces the same exactly result as a real experiment. Figure 3.31a shows the baseline and Figure 3.31b shows the line fitted in the difference measurements for a single simulation.

Figure 3.32 shows the difference calculations for one of the experiments using the basic model and maximum speeds of 1 and 20.

In Figure 3.32a, the difference between the two videos increases during the simulation and the value of the fitted line slope is $a = 0.1943$. On the other hand, in Figure 3.32b the difference almost remains constant, with line slope of $a = -0.0381$. Using the slope criteria, the simulation with maximum speed of 20 is more similar to the real experiments than the simulation using 1.

The next step is to identify the parameter that gives a line with a equals to 0. Using the slope measurements for three different experiments, each containing 15 simulations with different parameters, another line is fitted in the data and the best parameter is identified finding the value of the parameter which gives $a == 0$. Figure 3.33 shows the slope calculations for all simulations being used to extract the line.

This procedure is performed for each bacteria model in order to identify their best parameter configuration.

3.5 Model Evaluation Process

Having all tools being presented, it is possible to define a process to evaluate and enhance the simulator. For this, it is proposed the flow as in Figure 3.34.

Having the bacteria step response videos, the next step is evaluate the current available models. Thus, a simulation using the image setup is performed using all models with different parameters. The simulator already provides a feature to record videos checking for the bacteria swarm step response. With the video experiment and the simulation videos, the difference estimation tool is used in order to check which one has the closest behavior to what is seen in the reality.

In some cases, the parameters can be changed in order to reach more representative model. It may also be the case that new models should be created to get a lower difference.

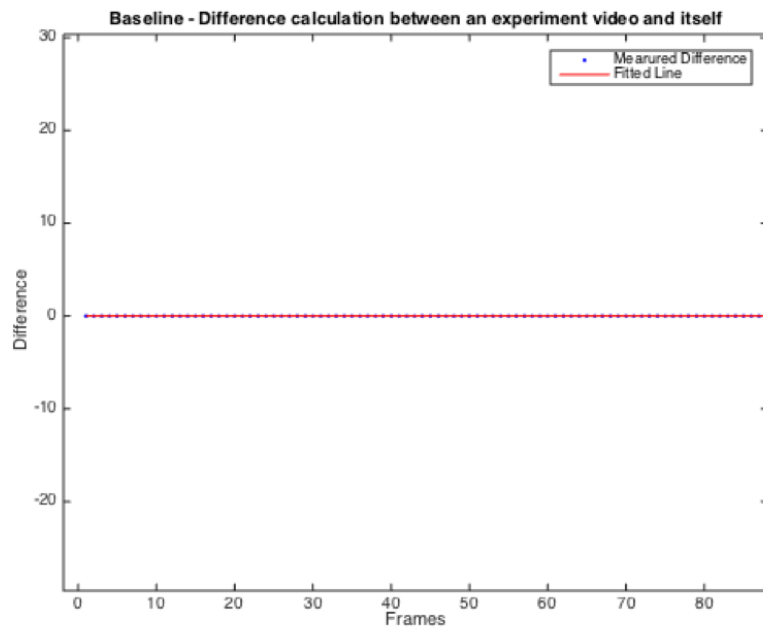
With the model set, the available controllers can be tested. The controller performance is calculated using the difference between the setpoint and the real position of the swarm during a simulation and the swarm dispersion while using the controller.

Other controllers can be created using this new model. Ideally, when testing it

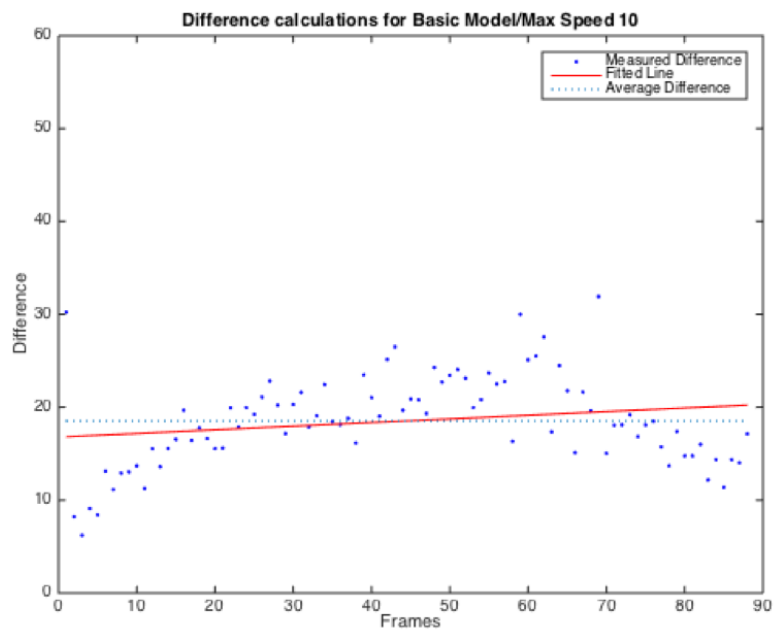
with the real bacteria, the behavior should be close to the observed in the experiments, as the controller was tested using the most similar bacteria model available in the simulator.

Finally, the cycle goes back to the experiments, where the real controller can be tested with real bacteria. For now there is not enough infrastructure on the microscopy to test the controllers using bacteria.

In the next chapter the results obtained using the proposed methodology are presented.



a)



b)

Figure 3.31. a) Baseline obtained comparing an experiment video to itself and b) the differences from the reference experiment calculated throughout the simulation is used to extract a line. It is expected that the smaller the line slope, the closer the video is to the reference.

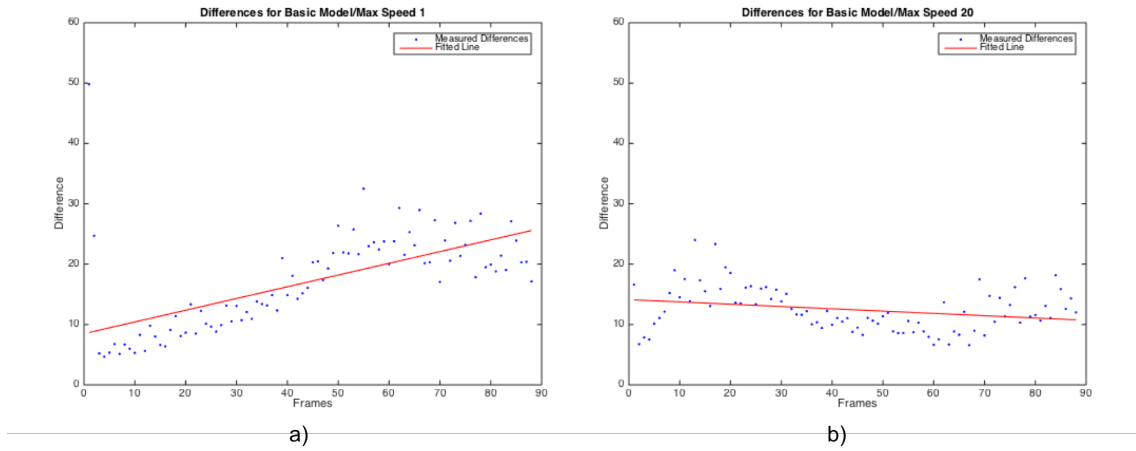


Figure 3.32. Difference calculations between the experiment video and the simulation using the basic model. (a) shows the result of one simulation with maximum speed of 1 (slope = 0.1943) and (b) another with maximum speed of 20 (slope = -0.0381). Note that, as the line slope is closer to 0 on the simulation with maximum speed 20 is more similar to the experiment.

Real Experiments

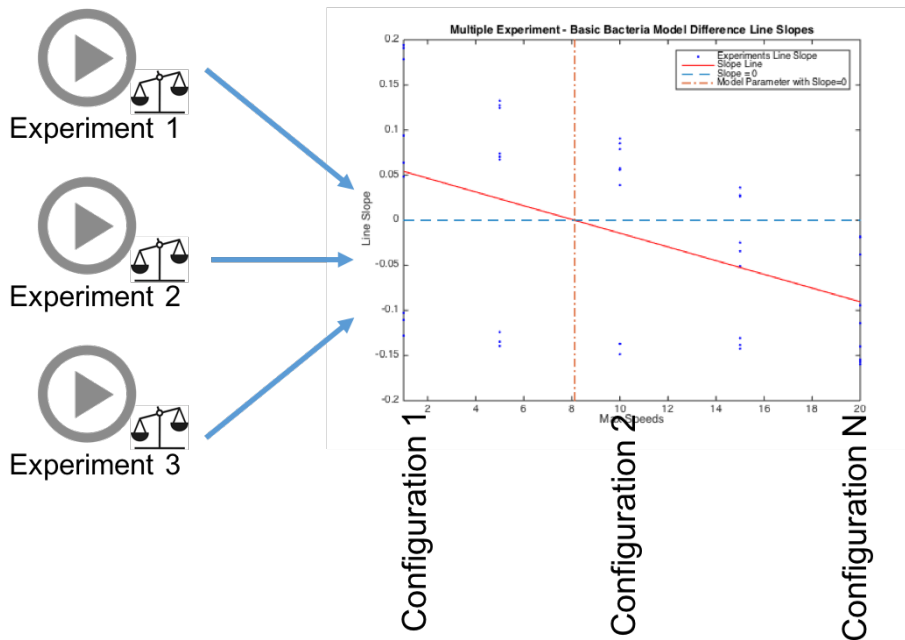


Figure 3.33. The line slopes for the different experiments and configurations are used to identify the parameter that gives a simulation which slope would be zero.

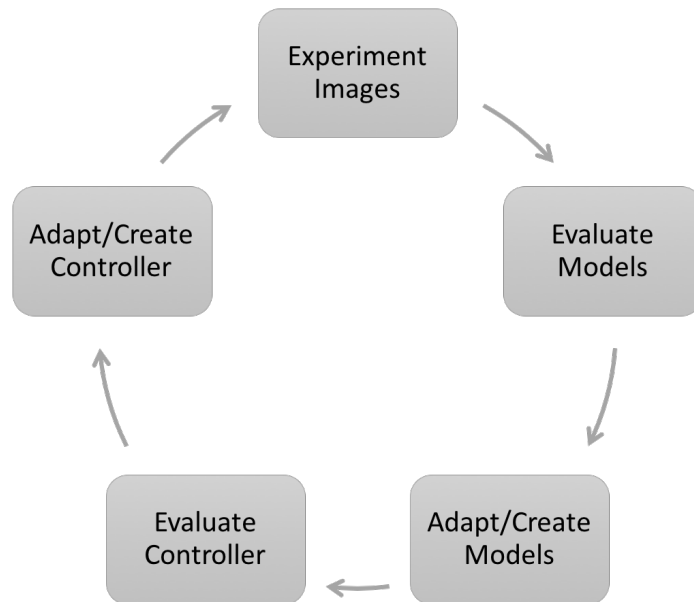


Figure 3.34. Simulator flow for bacteria models and controller enhancement

Chapter 4

Experiments and Results

This chapter presents the performed experiments and the analysis of the captured images.

4.1 Real Bacteria Experiments

During the project execution four experiments were performed using real bacteria. They are presented chronologically, showing their differences and how the process evolved.

4.1.1 Setup test and evaluation

The first experiment was done to validate the microscope setup and capture images of the *Magnetofaba itaipuensis*. The overall goals were:

1. Capture images using both 10x and 100x objectives.
2. Analyze setup robustness (stability, easy to change configurations and allow to reproduce experiments).
3. Observe bacteria behavior with manual magnetic field changes (using magnet).

Figure 4.1 shows a frame of one of the videos captured in the experiment, where the drop edge is used to accumulate the bacteria.

This experiment defined the test's procedures and some other setup configurations. It was observed that using *Magnetofaba itaipuensis* species the 100x objective is not recommended because the bacteria are too fast. So, they go out of the field of view

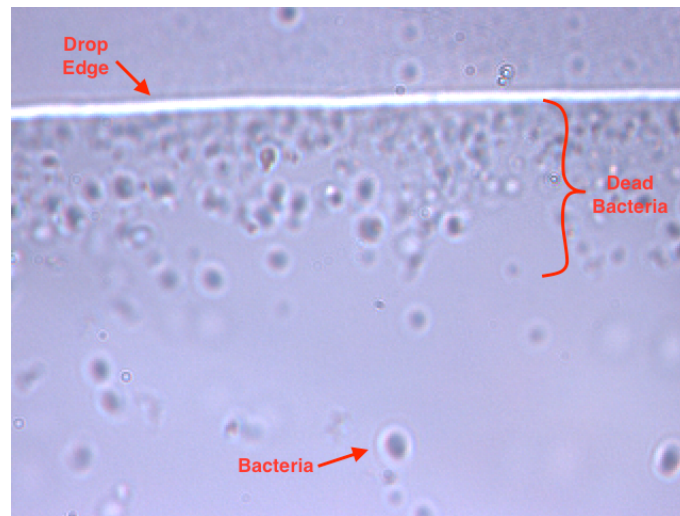


Figure 4.1. Image captured in the first experiment using the 100x objective. The bacteria moved toward the drop edge where they accumulate.

before the swarm formation. Besides this, the image using this objective is unstable, what makes it harder to reproduce experiments.

It was also observed that the bacteria response to the magnetic field stops about ten minutes after the sample is placed in the microscope. This was expected because the bacteria are microaerophile, so high concentration of Oxygen kills them. Figure 4.1 shows the bacteria agglomeration close to the border. Some of them are dead bacteria that are not responding to the magnetic field changes. This behavior is more explicit close to the border due to the higher Oxygen concentration.

Another important observation was that the life time of the bacteria after they are removed from the culture is about five days. After this, the bacteria collected from the samples do not respond to the magnetic field anymore.

4.1.2 Swarm observation and electronic circuit test

The goals of this experiment were:

1. Capture images using the 10x objective.
2. Observe the swarm formation on the drop border.
3. Test the electronic circuit that generates the magnetic field.

Using the same procedures established in the later experiment, this time the bacteria observed in the samples were not responding to the magnetic field. Figure 4.2 shows a bacterium with a different shape than the expected. Their behavior was

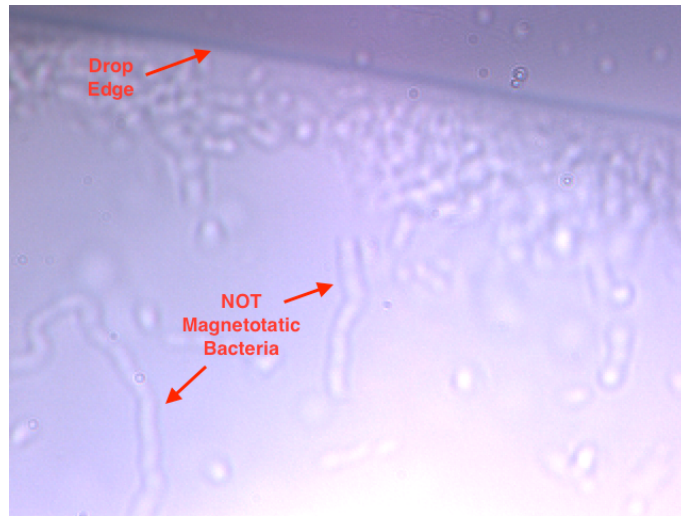


Figure 4.2. Image captured in the experiment of December/2015 using the 100x objective. No magnetotactic bacteria were observed in the samples. According to the researchers in UFRJ there were a contamination in the samples.



Figure 4.3. Magnetic field using the electronic system. In this image the coils generate a magnetic field B from the left to the right, as shown by the red arrows. Note that the compass aligns with the magnetic field lines.

aleatory and apparently not related to magnetic fields changes and the absence of magnetotactic bacteria was caused by a culture contamination.

Even without success on observing the magnetotactic bacteria, the electronic system to generate magnetic field was tested and validated using a compass. In this experiment, a small compass was placed between the coils and the current inverted being possible to observe its direction depending on the current configuration. Figure 4.3 shows the compass needle aligning itself with the magnetic field generated by the coils.

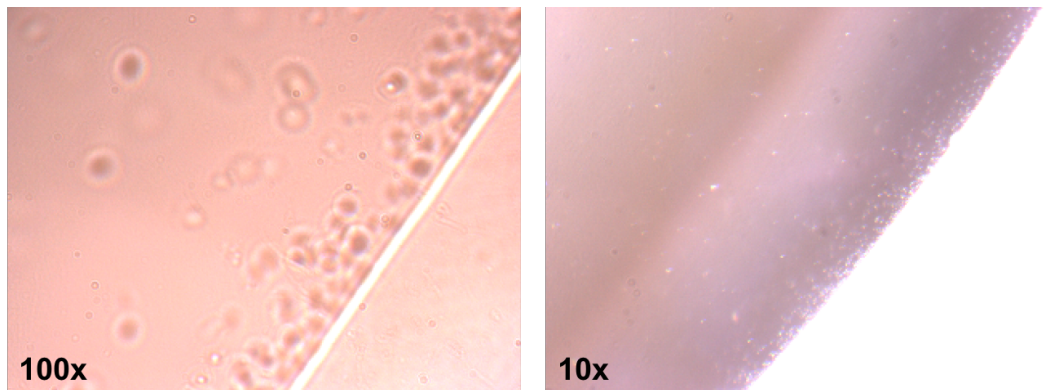


Figure 4.4. Image captured from the experiment performed in May/2016 using the $10x$ and $100x$ objectives. The $100x$ is more suitable for the experiments as the swarm is easily identified. Note the bacteria agglomeration in the drop edge.

4.1.3 Swarm observation

The goals of this experiment were:

1. Capture images using the $10x$ objective (from later experiment).
2. Observe the swarm formation on the drop border (from later experiment).
3. Observe bacteria behavior with the magnetic field being changed by the electronic system.
4. Check the feasibility of creating a magnetic field gradient using the coils.

The experiments took three consecutive days and it showed that the image of the bacteria swarm using the $10x$ objective was much more clear and suitable for the project than the image using the $100x$ objective. Figure 4.4 shows one frame of a video captured using the $10x$ objective in which the bacteria were agglomerated in the edge of the drop. The image using this objective is more stable and the swarm is easily identified. Besides this, it does not require oil to work, so the experiment procedures become faster and cleaner.

During the simulator development, it was considered the creation of a magnetic field gradient in order to agglomerate the swarm in any place inside the drop. For that, the magnetic field configurations presented on Figure 4.5 were tested on the available setup in order to verify the feasibility of this approach. In the figure, the arrows point the direction of the magnetic field. Figure 4.5a and 4.5b represents the regular setup, where the bacteria swarm navigates toward the drop edges and accumulates there. The approach presented in Figure 4.5c considers that the intensity of the magnetic field and

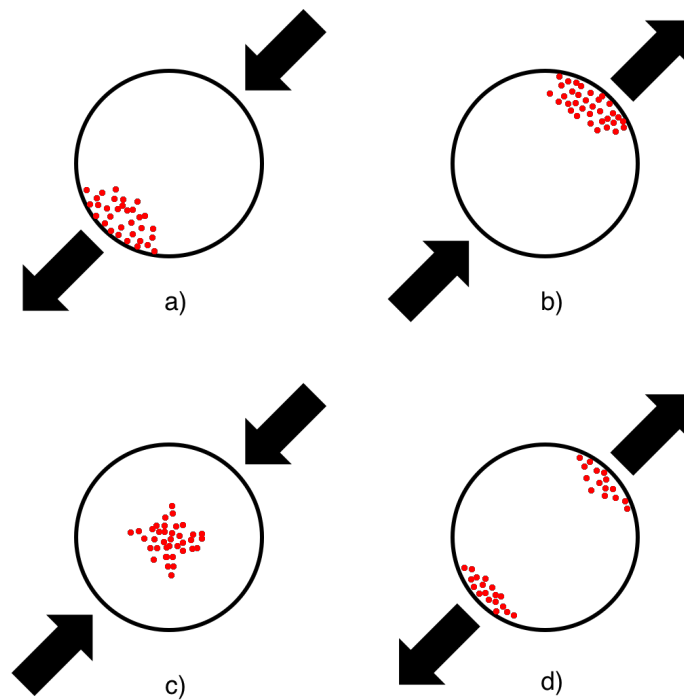


Figure 4.5. Expected bacteria formation applying different magnetic fields over the sample (arrow points to the North). (a) and (b) are the behavior seen in the previous experiments, (c) presents a situation where a gradient exists in the middle of the drop and (d) a situation where two swarms are created in the sample.

the distance from the sample are the same in both coils. This case, in theory, would create a magnetic field gradient that would bring the swarm to the center of the drop. In the last case of Figure 4.5d, as the magnetic field have opposite directions, ideally two swarms would appear.

All those combinations were tested, but situations presented in Figures 4.5c and 4.5d were not observed. In both cases, a single swarm appears in one of the edges of the drop. This can be explained by the fact that the setup is not precise, so it is not possible to be sure that the magnetic fields generated by the coils are the same (different currents, wire resistance, number of turns, etc) neither that the distance from the coils to the sample are the same.

Considering this, the magnetic field approach that considers the generation of a magnetic field gradient is not feasible with the current setup. To make this possible, it needs to be restructured to become more robust. For this, the support for the coils must be more stable, the coils fixed and the wire turns around the ferrite core determined. The distance between the coils and the sample must also be the same and the electronic circuit that generates the current more steady.

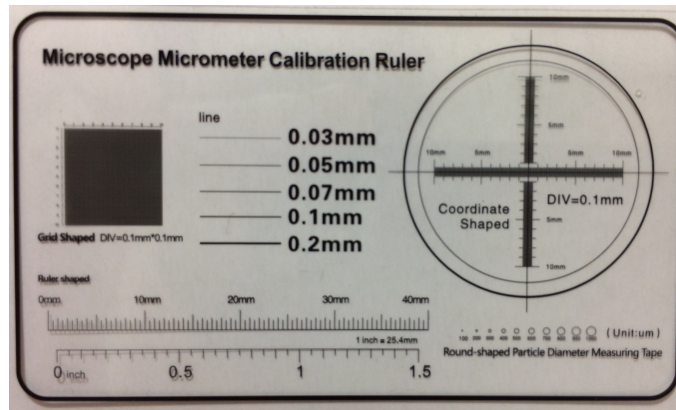


Figure 4.6. Calibration ruler used to extract the $\mu m/px$ relation. This ruler was part of a USB microscope purchased by the laboratory.

4.1.4 Camera calibration and step response

The last experiment was done after the difference estimation tool and activity methodology were established. The goals were:

1. Get a calibration for the camera.
2. Capture videos of the bacteria step response.

4.1.4.1 Calibration

The calibration for the acquired images used the calibration ruler shown in Figure 4.6. This ruler contains lines and circles with fixed sizes and it is used to extract the $\mu m/pixel$ relation for the setup. In this case, the calibration was performed using images from the lines with different sizes and the $10x$ objective.

Using *imageJ* tool [Abràmoff et al., 2004], the width of the lines in the captured images were measured twice in different parts of the image to reduce measurement errors. Figure 4.7 shows the $0.1mm$ line and the places where the measurements were done.

Table 4.1 presents the results obtained using images captured from lines of $0.03mm$, $0.05mm$, $0.07mm$, $0.1mm$ and $0.2mm$. The average calibration obtained was $0.8015\mu m/px$ with standard deviation of 0.053 .

Analyzing the images with bacteria, the bacterium size in pixels goes from one to three pixels. Using the calibration information, the bacteria size in the images goes from $0.8015\mu m$ to $2.4045\mu m$, what is close to the expected ($1.4 \pm 0.3\mu m$) [Morillo et al., 2014].

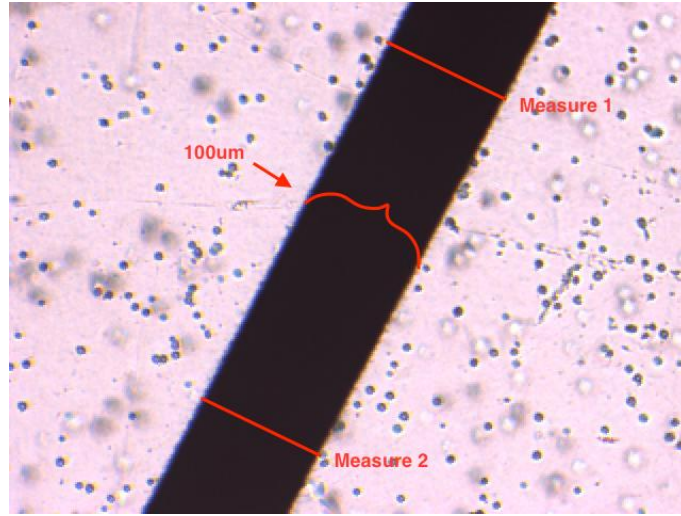


Figure 4.7. Captured image of the 0.1mm line in the calibration rule. Using *imageJ* tool, two measures are performed in order to reduce the error.

Table 4.1. Camera Calibration

<i>Size(μm)</i>	<i>Measure 1(px)</i>	<i>Measure 2(px)</i>	<i>Calibration ($\mu\text{m}/\text{px}$)</i>
30	41.42	40.31	0.7341
50	63.25	64.19	0.7846
70	87.52	90.10	0.7881
100	121.44	122.40	0.8202
200	228.55	225.66	0.8806
		Average	0.8015

4.2 Activity Analysis

The videos of the bacteria step response are the base of the activity analysis. They were performed using the methodology defined previously, where the bacteria swarm is first accumulated in the border and then the video is captured right after the field is inverted. Figure 4.8 shows the video from $t = 0.0\text{s}$ to $t = 4.16\text{s}$. Note that the bacteria swarm follows the magnetic field direction (indicated by the red arrow) and eventually goes out of the field of view.

For the same sample and the same setup, the procedure is done for about 15 minutes or until the bacteria stop responding. This way, the bacteria activity can be measured and analyzed considering the time the sample is exposed to Oxygen. As the bacteria are microaerophile, it is expected a decrease on their activity.

Figure 4.9a shows the activity of the first captured video, right after the sample is in the microscope. In the graph, the point (1) represents the time the swarm starts

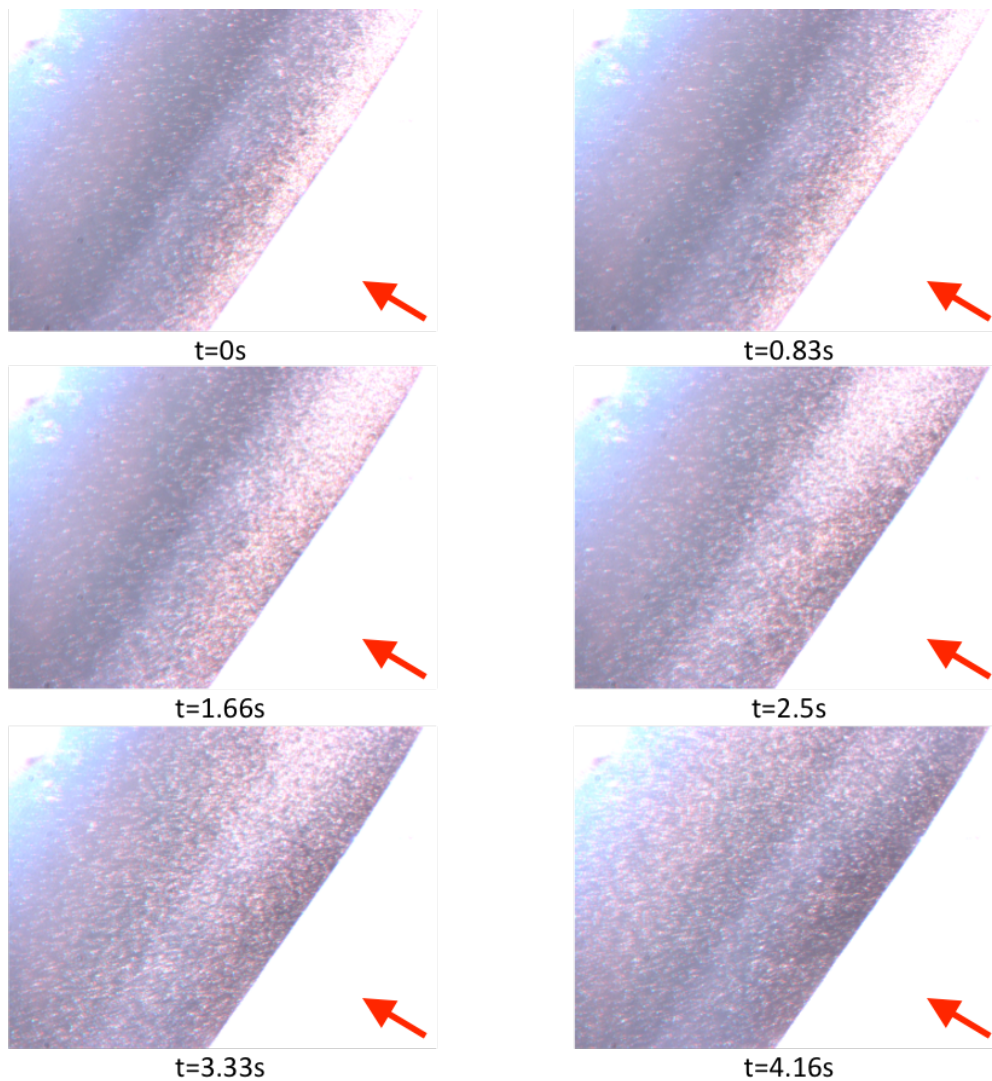


Figure 4.8. Step response video taken right after the magnetic field is inverted. In time $t = 0$ the bacteria agglomerated on the border. After that they are oriented by the new magnetic field and eventually leave the field of view. The red arrow indicates the magnetic field direction.

responding to the magnetic field inversion. Then, it moves and the activity reaches a maximum (2) where the whole swarm is moving. Then, the activity decreases because the swarm starts going out of the field of view. Point (3) represents the last activity measured when part of the swarm has already left the image.

The activity average is related to the amount of the bacteria in the experiment responding to the magnetic field. Besides that, during the analysis, it was observed

that it is possible to approximate the activity during the step response by a Gaussian function. This function is used to obtain the frame in which the maximum activity is observed, which relates to how fast the swarm responds to the magnetic field.

For the same experiment, Figure 4.9b presents the activity analysis of the video captured approximately 15 minutes after the sample is placed in the microscope. A visual inspection of the video shows that there is no apparent activity in it because the bacteria have already died due to the Oxygen exposure. Note that the Gaussian function does not represent the activity seen in the graph. The measured activity in this case may be due to noise in the image and small brightness variations. This behavior was seen in videos captured after the sample were exposed to Oxygen for about 700 seconds (approximately 11 minutes). This way, in further analysis, videos captured after this time limit are not considered.

Considering both graphs presented in Figure 4.9, it is possible to conclude that, if the video used to create the graph in Figure 4.9a had continued, giving time for the whole swarm to disappear from view, the activity value would eventually reach the value of the graph in Figure 4.9b, whose average is $0.83 * 10^4$.

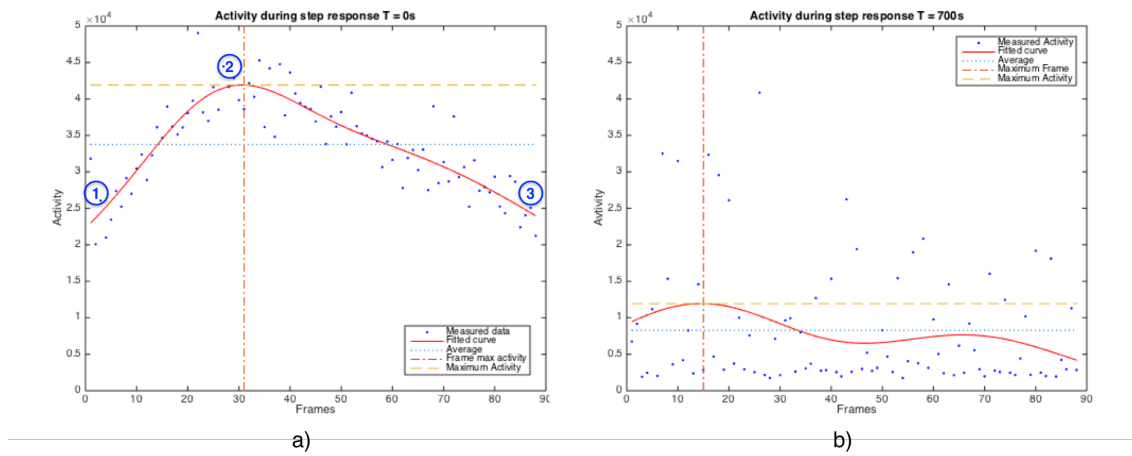


Figure 4.9. Graph (a) presents the activity measured during the first step response captured video. Point (1) indicates the moment the swarm starts responding to the opposite magnetic field. (2) shows the maximum activity observed, when the whole swarm is moving. (3) is the moment that part of the swarm leaves the image. Graph (b) presents the same analysis considering a video captured 15 minutes after the start of the experiment, without any visual movement. Note the low activity average ($0.83 * 10^4$).

Figure 4.10 presents the procedure performed to extract the information from a single experiment. The activity is calculated to all videos belonging to the experiment and then the data was joined. This analysis does not consider videos captured after 11

minutes the sample is exposed.

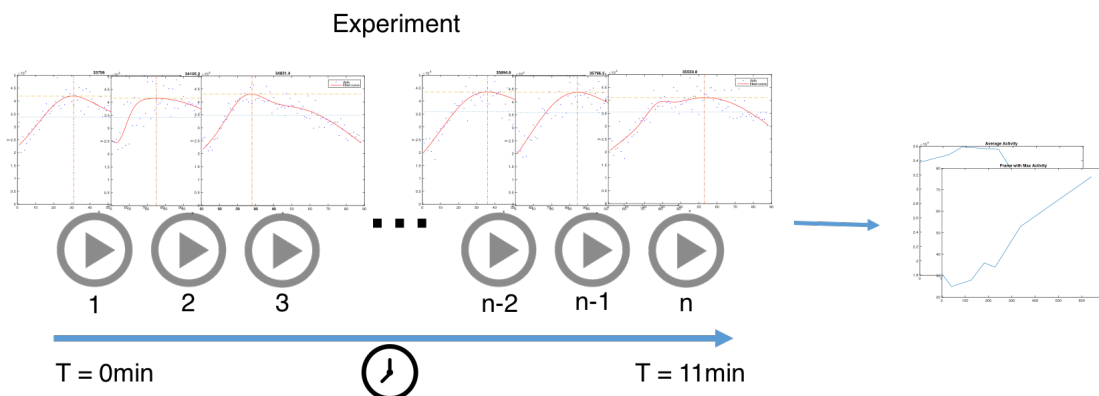


Figure 4.10. The activity in each video is calculated separately and then joined in order to observe the relation between the average activity and the frame with maximum activity and time.

Using the average activity in each video and the frame where the maximum activity was observed it was possible to plot the charts in Figure 4.11.

Figure 4.11a shows the average activity measured on a single experiment containing seven videos with different exposure times. As expected, the higher the exposure time the lower the average activity observed.

The second information extracted from the analysis was the frame in which the maximum activity in the Gaussian function occurred. Considering that the bacteria dies after some time, it is fair to conclude that the more the sample is exposed to Oxygen the later the bacteria will respond to the magnetic field changes. This behavior is seen in 4.11b.

As presented in Figure 4.12, this analysis was done in four experiments with different setups. Then, the data is joined in order to observe in more than one experiment how the Oxygen exposure affects the average activity and the frame with maximum activity.

Figure 4.13a shows the relation between the average activity and exposure time. Note that there is a tendency, but data are spread. This can be explained by the fact that the average activity is directly related to the number of bacteria in the sample. The higher the amount of bacteria in it the more activity will be observed. As each experiment is performed with a different bacteria sample, the amount of bacteria in each is different from the other, what explains the variability in the values.

On the other hand, the graph in 4.13b shows the frame with maximum activity regarding time. It is possible to use this data to extract the Equation 4.1 relating the

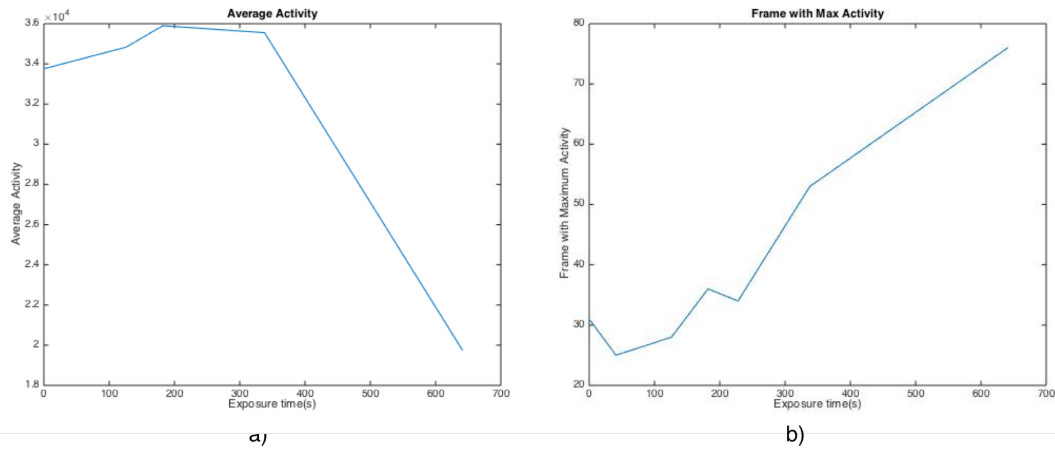


Figure 4.11. Figure (a) shows the maximum bacteria activity measured on videos captured with different exposure times and (b) shows the frame in which the maximum activity occurred in each video regarding the exposure time.

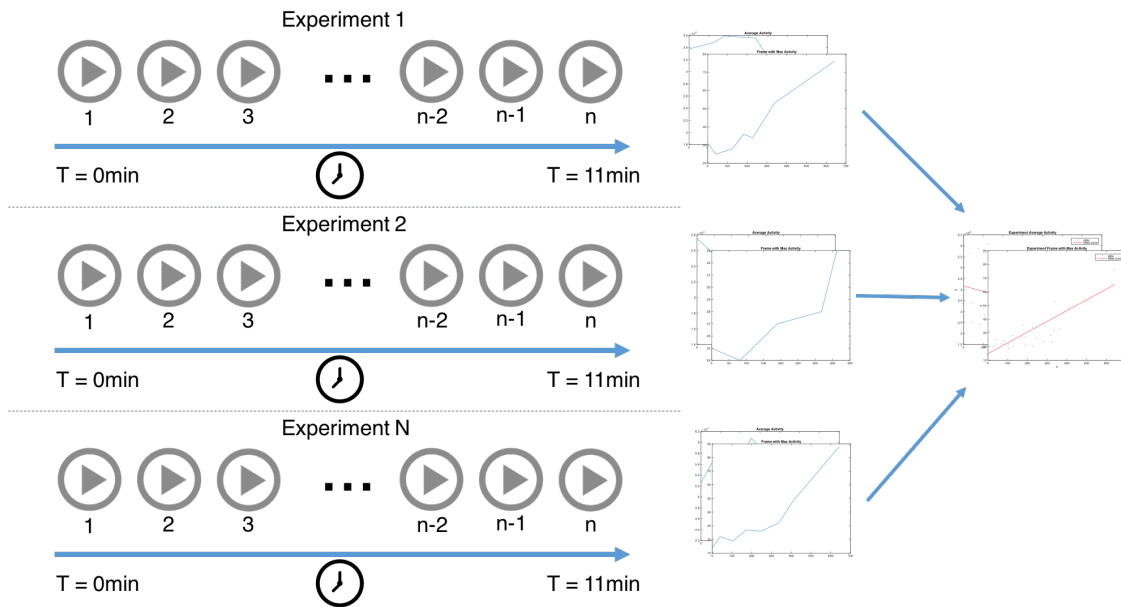


Figure 4.12. Each experiment is processed separately and the data joined in order to observe the relation between the average activity and the frame with maximum activity.

frame where the maximum activity occurs to the time the sample is exposed. It is important to highlight that this equation is only valid for times between 0 and 700 seconds, where the observed bacteria behavior is predictable.

$$f(t) = 0.078t + 14.89 \quad \forall t \in [0, 700] \tag{4.1}$$

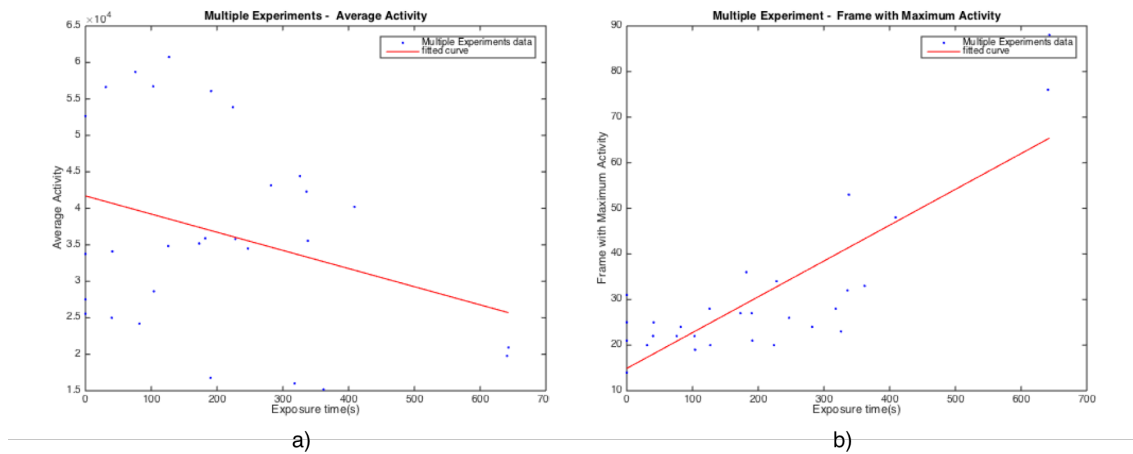


Figure 4.13. Using data from multiple experiments the graph in (a) shows the maximum bacteria activity on different exposure times and (b) the graph that relates the frame with maximum activity and time.

The activity analysis showed that the behavior of the *Magnetofaba itaipuensis* depends on the time that it is exposed to Oxygen and this can be used to define how the bacteria can be used in future applications. Besides this, it was possible to define a time limit that the sample can be used in the experiments before the losing their magnetotaxis capability.

4.3 Simulator Validation

To identify the best model and the parameters to be used in the simulations it is used the methodology presented before.

4.3.1 Best Model Identification

Using the overall average difference obtained on the simulations with different configurations is possible to compare which bacteria model is more similar to the real experiments. Figure 4.14a shows the overall average difference for the simulations using the basic bacteria model, whose value is 15.5902. Figure 4.14b shows the same calculation performed on the simulations using the adapted bacteria model, whose value is 14.6310.

As it is possible to see in the graphs, by the fact that the values are close, the overall difference calculation is not enough to define the best model to be used in the simulations. For this reason it is calculated the standard deviation of the data. On the basic bacteria model data, the standard deviation is 2.1296, while on the adapted

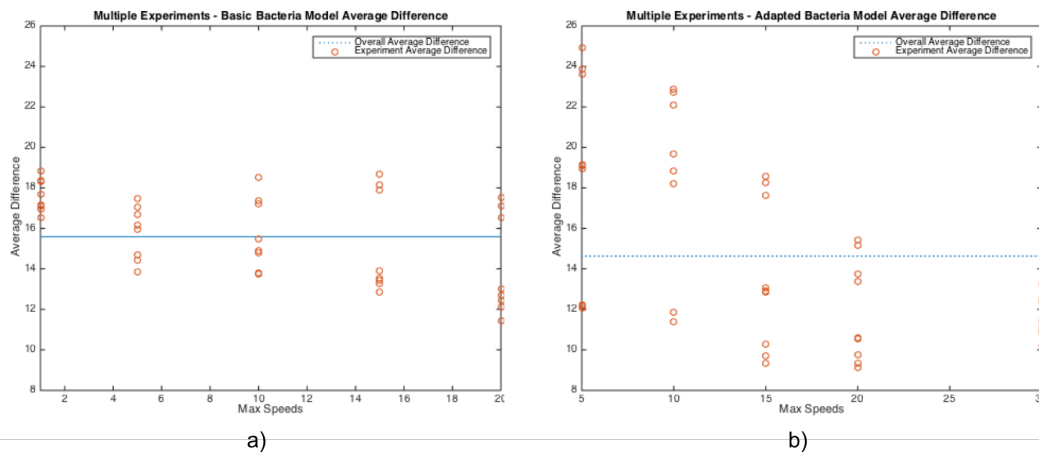


Figure 4.14. a) Overall average difference calculation for simulations using the basic bacteria model and b) using the adapted model. As the values are really close it is used the data standard deviation to define the best model.

model the standard deviation is 4.6621. For this reason the simulations using the basic bacteria model should be used.

4.3.2 Best Parameters Identification

Even though it was identified that the basic bacteria model is closer to the experiments, next it is presented the results to obtain the best parameters for simulations using each bacteria model.

4.3.2.1 Basic model

Using the Basic bacteria model, the following maximum speeds were used to generate simulation videos: 1, 5, 10, 15 and 20 units. For each of those configurations, three videos were generated and compared with the reference experiment video.

The graph in Figure 4.15 presents the slopes of the lines obtained on the differences calculations for all different simulations.

Analyzing Figure 4.15 it is possible to identify that the optimal maximum speed to obtain the the most similar simulation is 8.1181, which corresponds to the parameter that gives a line with slope equals to zero.

4.3.2.2 Adapted model

The same procedure is performed using the adapted bacteria model. Due to its different behavior, the maximum speeds used were: 5, 10, 15, 20 and 30. Figure 4.16 shows the

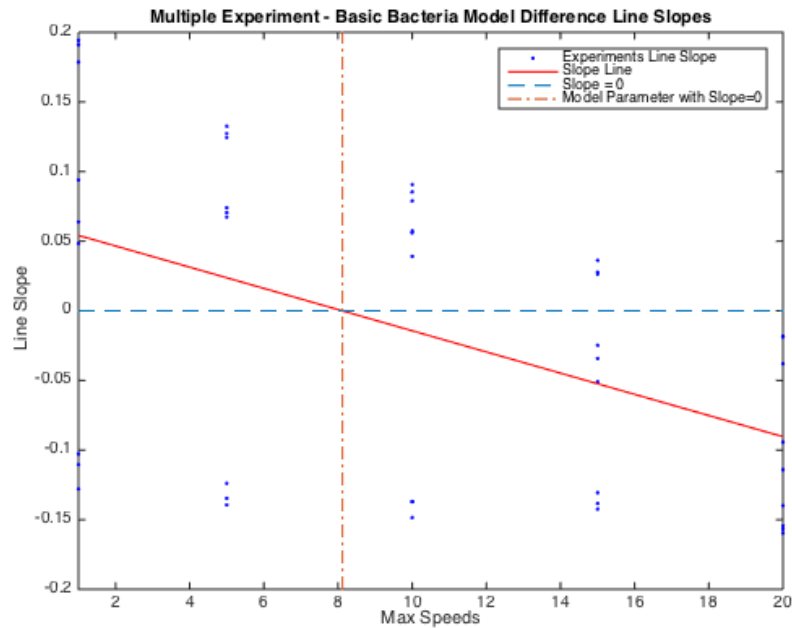


Figure 4.15. Line slope calculations for the basic bacteria model using multiple experiments as reference. The bacteria maximum speed that gives a line slope equals to zero is 8.1181.

line slope calculation performed using all simulations with the adapted bacteria model. The best maximum speed to be used is 8.9937.

So, for each bacteria model, the parameters that make the simulation as close as possible to the real experiments are:

- Basic bacteria model: Maximum Speed = 8.1181
- Adapted bacteria model: Maximum Speed = 8.9937

For the reasons explained before, the simulations performed in the next experiments will use the basic bacteria model with maximum speed of 8.1181.

4.4 Simulator Experiments

Considering that the best model and its parameter is defined, some experiments using the simulator could be performed.

The first one was to accumulate the bacteria in one of the corners of the image. In this case, the four borders limit the bacteria movement and the grid size is 640×480 . Figure 4.17 shows the bacteria movement when the magnetic field direction points to

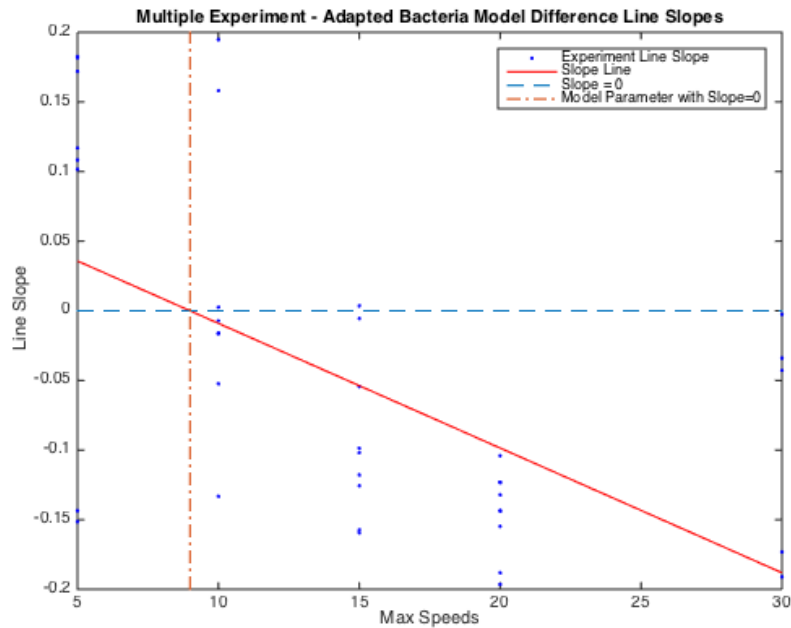


Figure 4.16. Line slope calculations for the adapted bacteria model using multiple experiments as reference. The bacteria maximum speed that gives a line slope equals to zero is 8.9937.

the top left corner. Comparing it to the Figure 4.8 and considering that the grid size is the same, it is possible to see that the swarm behavior is close, mainly regarding the time it reaches the corner (4s).

Next, the controller validation is presented using the obtained models parameters.

4.4.0.1 Controller

The Fuzzy Controller must also be validated to verify its applicability in the real experiments. For that, using the parameters discovered previously, an experiment was performed in order to observe the controller robustness. In this case, one of the videos of the experiments is used as reference, defining a grid of 640×480 pixels. For the simulation it is defined the magnetic field upper limit of 5 and 500 bacteria in the sample. The goal of such experiments was observe the distance between the swarm center and the setpoint and the dispersion of the swarm over the time.

In this experiment, the bacteria are accumulated in the edge of the drop, creating the swarm. Then, the setpoint is defined to the center of the grid and the controller enabled. Figure 4.18 shows the frames of the experiment using the basic bacteria model. Note that after some time the swarm dispersion gets bigger.

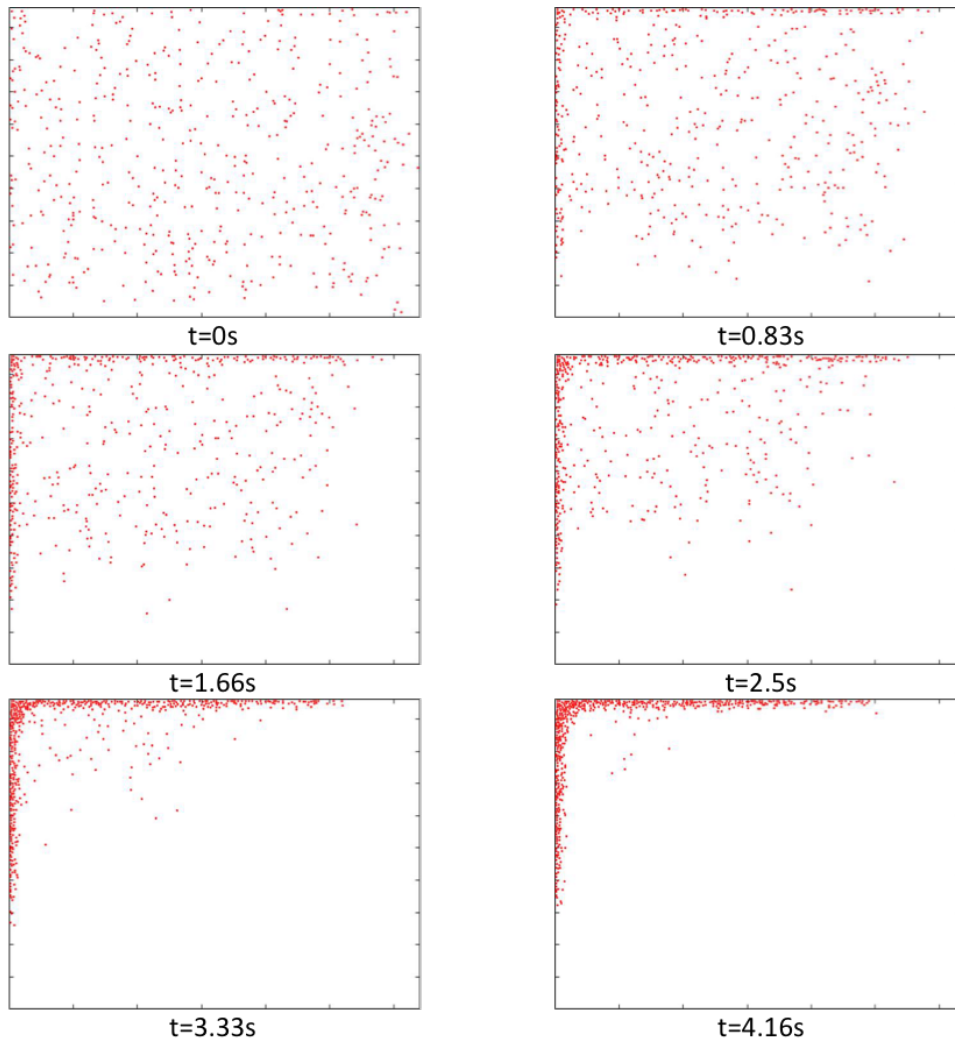


Figure 4.17. Simulation agglomerating bacteria in the top left corner of the image.

A similar experiment was performed using the best parameters of the adapted model in order to compare the distances between the swarm center and the dispersion of it using the difference models. Figure 4.19 shows the distance between the center of the swarm and the setpoint over the iterations. Note that the basic model presents a much faster convergence compared to the adapted model.

The second observed behavior was the dispersion of the swarm over the iterations. This value was obtained calculating the standard deviation of the bacteria position in the swarm. The higher the value, the more disperse is the swarm. Figure 4.20 shows the dispersion observed using both models. The dispersion is tightly related to the

randomness of the model, characteristic more present in the adapted bacteria model. As expected, the dispersion on it is higher than the one using the basic model.

To reduce the dispersion, the controller may be enhanced adding more fuzzy states. This would allow the system to apply a more refined magnetic field value over the sample, thus reducing the gap between the swarm center and the setpoint.

The tool also allows the controller to use a set of predefined setpoints to make the swarm to travel in a specified route. This is useful to show that, after the bacteria is accumulated, it is possible to make the swarm goes to specific locations without losing the control of it. It is important to highlight that this is only feasible when the swarm is in the field of view of the microscope, as the controller requires the visual input to actuate over the system.

Finally, this experiment showed that, due to the smaller dispersion and faster response, the developed controller fits better the basic bacteria model, which is the model with lowest differences compared to the real experiments. If a better model is identified, the fitness of the current controller must be evaluated again and it may be the case to adapt it to the new behavior.

In the next chapter the conclusions of this project are presented, together with the future works related to it.

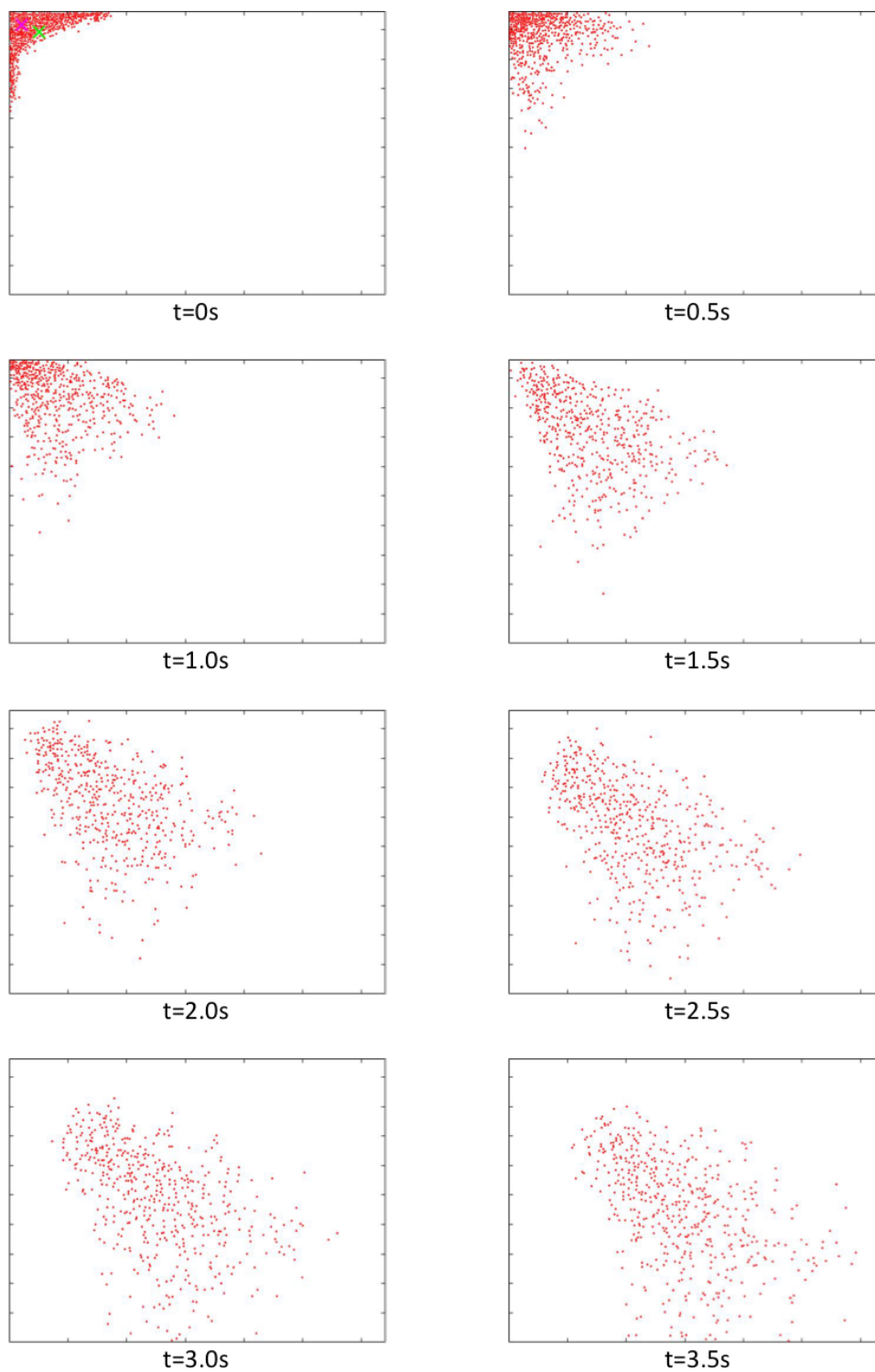


Figure 4.18. Frames showing the controller acting over the swarm position with the setpoint being the center of the grid. Note the dispersion of the swarm over the time.

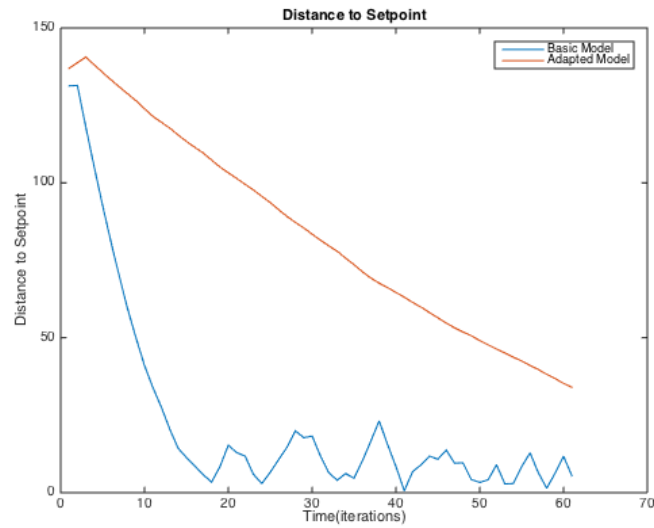


Figure 4.19. Distance between the swarm's center and the objective over the time (iterations).

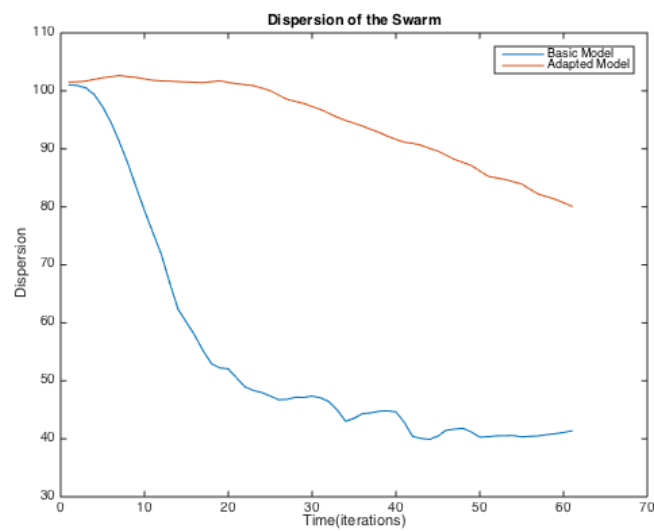


Figure 4.20. Dispersion of the bacteria over the time (iterations).

Chapter 5

Conclusions and Future Works

This project imposed many challenges for its realization, like building a physical setup that would allow the experiments to be performed in an organized and reproducible way. In this phase, besides the setup, it was necessary to understand the optics behind the system and define the best illumination strategies to use in order to achieve the best images for such setup.

The developed microscope is capable to capture stable videos and allows different image resolutions. The setup is robust enough to be used in new experiments but the electronic system still needs to be reviewed in order to allow more reliable magnetic field configurations.

The bacteria availability is still a problem regarding the experiments, but as we are trying to cultivate the *Magnetofaba itaipuensis* inside UFMG, in the near future experiments may not be that hard to perform. Besides this, this bacteria is being considered for some synthetic biology studies so its culture may be used in other researches as well.

Another challenge was to build a computer system to simulate the bacteria behavior based only on the visual observations done during the experiments. Though some papers presented a mathematical model for the magnetotactic bacteria [Khalil et al., 2013] [Ma et al., 2012] [Bahaj and James, 1993], no other work has used the *Magnetofaba itaipuensis* species as the basis for the work.

The last big challenge was to correlate the experiments done using the simulator to the real experiments. The methodology used to validate the mathematical models is also presented in some papers, but they count with a more robust setup and more availability of bacteria. In this thesis, the methodology is defined in order to identify the best model between the available ones, all of them created based on visual observations and some definitions found in papers. This does not mean that there is no other model

that represents better the bacteria behavior.

The simulator validation has shown that the basic bacteria model with maximum speed of 8 simulation units is the configuration that better represents the real bacteria behavior. Besides the fact that the difference is smaller than in the other models, the controller evaluation showed that it is also the best configuration be used with the fuzzy controller. In this case, the bacteria swarm converges faster to the setpoint and the dispersion is smaller.

Regarding the bacteria activity, the expected behavior was observed in the experiments and proved that the methodology can be used to measure and estimate how a sample exposed to Oxygen will behave over the time. The results shows that the bacteria do not last more than ten minutes after removed from the sample and this effects how the experiments should be performed. This information can be used in future experiments to discard samples after some time and even to enhance the simulator models.

As future works, more models can be created and the controller tested using real bacteria. The setup imposes some restrictions that must be trespassed before going further. The electronic setup used to create magnetic field is not as stable as expected and is not precise enough to generated the required field for some study cases. The optics can also be enhanced, maybe with a better microscope or using other techniques such as phase-contrast or fluorescence microscopy.

There are also other types of controllers that can be implemented and tested using the simulator but, as said, in order o validate it on the real system, some improvements on the electronic and in the optics part must be done.

Finally, though the nanorobotics topic seems interesting, there are some ethical discussions that must take place in order to define what is “right” or “wrong” when talking about using nanorobots to perform tasks. In this work it was showed the feasibility to use the *Magnetofaba itaipuensis* in the nanorobotics field but to define how it will or should be used is part of another debate.

Bibliography

- Abràmoff, M. D., Magalhães, P. J., and Ram, S. J. (2004). Image processing with imagej. *Biophotonics international*, 11(7):36--42.
- Akyildiz, I., Pierobon, M., Balasubramaniam, S., and Koucheryavy, Y. (2015). The internet of bio-nano things. *IEEE Communications Magazine*, 53(3):32--40.
- Akyildiz, I. F. and Jornet, J. M. (2010). The internet of nano-things. *IEEE Wireless Communications*, 17(6):58--63.
- Asimov, I. (2011). *Fantastic voyage*. Bantam.
- Bahaj, A. and James, P. (1993). Characterisation of magnetotactic bacteria using image processing techniques. *IEEE Transactions on Magnetics*, 29(6):3358--3360.
- Bahaj, A., James, P., and Moeschler, F. (1998). Low magnetic-field separation system for metal-loaded magnetotactic bacteria. *Journal of magnetism and magnetic materials*, 177:1453--1454.
- Bazyllinski, D. A., Garratt-Reed, A. J., and Frankel, R. B. (1994). Electron microscopic studies of magnetosomes in magnetotactic bacteria. *Microscopy research and technique*, 27(5):389--401.
- Bazyllinski, D. A. and Schübbe, S. (2007). Controlled biomineralization by and applications of magnetotactic bacteria. *Advances in applied microbiology*, 62:21--62.
- Callaghan, E. E. and Maslen, S. H. (1960). The magnetic field of a finite solenoid.
- Cebron, D. (2015). Magnetic fields of solenoids/magnets - file exchange - matlab central.
- Crichton, M. (2002). *Prey: a novel*.
- de Lima, G. L., Neto, O. P. V., et al. (October 2013). Nano e microrrobótica com bactérias flageladas. *XI SBAI*.

- Debevec, P., Bregler, C., Cohen, M., Mcmillan, L., Sillion, F., and Szeliski, R. (2000). Image-based modeling, rendering, and lighting.
- DeLong, E. F., Frankel, R. B., and Bazylinski, D. A. (1993). Multiple evolutionary origins of magnetotaxis in bacteria. *Science*, 259(5096):803--806.
- Derby, N. and Olbert, S. (2010). Cylindrical magnets and ideal solenoids. *American Journal of Physics*, 78(3):229--235.
- Dorf, R. C. and Bishop, R. H. (1998). Modern control systems.
- Halliday, D., Resnick, R., and Krane, K. S. (1992). *Physics. Vol. 3*. Wiley.
- Horn, B. K. and Schunck, B. G. (1981). Determining optical flow. *Artificial intelligence*, 17(1-3):185--203.
- Khalil, I. S., Pichel, M. P., Abelmann, L., and Misra, S. (2013). Closed-loop control of magnetotactic bacteria. *The International Journal of Robotics Research*, 32(6):637--649.
- Kimball, J. W. (2011). Taxes. <http://users.rcn.com/jkimball.ma.ultranet/BiologyPages/T/Taxes.html>. Accessed: 2016-11-20.
- Lawrence, G. R. (1963). *Machine perception of three-dimensional solids*. PhD thesis, Ph. D. Thesis, Massachusetts Institute of Technology, Cambridge, MA, USA.
- Lee, H., Purdon, A. M., Chu, V., and Westervelt, R. M. (2004a). Controlled assembly of magnetic nanoparticles from magnetotactic bacteria using microelectromagnets arrays. *Nano letters*, 4(5):995--998.
- Lee, H., Purdon, A. M., and Westervelt, R. M. (2004b). Micromanipulation of biological systems with microelectromagnets. *IEEE Transactions on magnetics*, 40(4):2991--2993.
- Levinthal, C. (1966). *Molecular model-building by computer*. WH Freeman and Company.
- Ma, Q., Chen, C., Wei, S., Chen, C., Wu, L.-F., and Song, T. (2012). Construction and operation of a microrobot based on magnetotactic bacteria in a microfluidic chip. *Biomicrofluidics*, 6(2):024107.

- Martel, S. (2006). Towards mri-controlled ferromagnetic and mc-1 magnetotactic bacterial carriers for targeted therapies in arteriolo-capillary networks stimulated by tumoral angiogenesis. In *Engineering in Medicine and Biology Society, 2006. EMBS'06. 28th Annual International Conference of the IEEE*, pages 3399--3402. IEEE.
- Martel, S., Felfoul, O., Mathieu, J.-B., Chanu, A., Tamaz, S., Mohammadi, M., Mankiewicz, M., and Tabatabaei, N. (2009a). Mri-based medical nanorobotic platform for the control of magnetic nanoparticles and flagellated bacteria for target interventions in human capillaries. *The International journal of robotics research*, 28(9):1169--1182.
- Martel, S., Mathieu, J.-B., Felfoul, O., Macicior, H., Beaudoin, G., Soulez, G., and Yahia, L. (2004). Adapting mri systems to propel and guide microdevices in the human blood circulatory system. In *Engineering in Medicine and Biology Society, 2004. IEMBS'04. 26th Annual International Conference of the IEEE*, volume 1, pages 1044--1047. IEEE.
- Martel, S. and Mohammadi, M. (2010). Using a swarm of self-propelled natural micro-robots in the form of flagellated bacteria to perform complex micro-assembly tasks. In *Robotics and Automation (ICRA), 2010 IEEE International Conference on*, pages 500--505. IEEE.
- Martel, S., Mohammadi, M., Felfoul, O., Lu, Z., and Pouponneau, P. (2009b). Flagellated magnetotactic bacteria as controlled mri-trackable propulsion and steering systems for medical nanorobots operating in the human microvasculature. *The International journal of robotics research*, 28(4):571--582.
- Martel, S., Tremblay, C. C., Ngakeng, S., and Langlois, G. (2006). Controlled manipulation and actuation of micro-objects with magnetotactic bacteria. *Applied Physics Letters*, 89(23):233904.
- Mendes, E. (2012). Modelagem matemática. Class Slides.
- Moore, B. L., Pyeatt, L. D., and Doufas, A. G. (2009). Fuzzy control for closed-loop, patient-specific hypnosis in intraoperative patients: A simulation study. In *2009 Annual International Conference of the IEEE Engineering in Medicine and Biology Society*, pages 3083--3086. IEEE.
- Morillo, V., Abreu, F., Araujo, A. C., de Almeida, L. G., Enrich-Prast, A., Farina, M., de Vasconcelos, A. T., Bazylinski, D. A., and Lins, U. (2014). Isolation, cultivation and genomic analysis of magnetosome biomineralization genes of a new genus

- of south-seeking magnetotactic cocci within the alphaproteobacteria. *Intracellular biomineralization in bacteria*, page 23.
- Nascimento, E. (2015a). Digital image processing. Class Slides.
- Nascimento, E. (2015b). Hough transform. Class Slides.
- Nascimento, E. (2015c). Optical flow - ii. Class Slides.
- Pele, O. and Werman, M. (2010). The quadratic-chi histogram distance family. In *European conference on computer vision*, pages 749--762. Springer.
- R. Fisher, S. Perkins, A. W. and Wolfart, E. (2016). Gaussian smoothing.
- Silveira, T. S. and Lins, U. (2007). Bactérias magnetotáticas. *Boletim da Sociedade Brasileira de Limnologia*, 36(1).
- Simoës, M. G. (2010). Introduction to fuzzy control. *Golden, Colorado, USA: Colorado School of Mines-Engineering Division*.
- Sugeno, M. (1985). *Industrial applications of fuzzy control*. Elsevier Science Inc.
- Szeliski, R. (2010). *Computer vision: algorithms and applications*. Springer Science & Business Media.
- Trucco, E. and Verri, A. (1998). *Introductory techniques for 3-D computer vision*, volume 201. Prentice Hall Englewood Cliffs.
- University, G. S. (2016). Hyperphysics.
- Wikimedia Commons (2016). Wikimedia commons.
- Yan, L., Zhang, S., Chen, P., Liu, H., Yin, H., and Li, H. (2012). Magnetotactic bacteria, magnetosomes and their application. *Microbiological research*, 167(9):507-519.

Appendix A

Microscope Setup

One open microscope was build from scratch, using the material described bellow.

- From ThorLabs®:
 - 3 Mounting Posts - P350
 - 3 Posts Base - PB2
 - 4 Posts Clamps - C1501
 - 1 Right-Angle Mounting Plate - AP90
 - 5 Universal Post Holder - UPH2
 - 2 Cage Plate - CP06
 - 4 Optical Post - TR50
 - 1 Broadband Dielectric Mirror - BB1-E02
 - 1 Bi-Convex Lens, $f = 150.0$ mm - LB1437
 - 1 Aluminum Breadboard, 600 mm x 900 mm - MB6090
- From Newport®:
 - 2 Double-Row Ball Bearing Linear Stage - UMR8.51
 - 2 Standard Resolution Micrometer - BM17.51
 - 2 Double-Row Ball Bearing Linear Stage - UMR5.25
 - 2 Standard Resolution Micrometer - BM11.25
- Nikon® objective lenses:
 - CFI 10x

– CFI Plan Apo VC 100X Oil

The objective lens support and the acrylic board for the sample were done exclusively for this setup. Besides this, it uses a LED Lamp 10W with white color light and a Dragonfly 2 camera connected to a computer through Thunderbolt port. It uses Windows 7 due to the programs compatibility.

Appendix B

Background review

B.1 Computer Vision

Since in this thesis many algorithms and concepts of Computer Vision are used, this section presents a brief review for a better understanding of our methodology.

The idea of Computer Vision is to extract a model from one or more images of a scene using a real camera (Figure B.1). This model may contain high level information, such as number of people in the scene, object geometry or even recognize faces and objects [Szeliski, 2010].

The formation of the image starts when the scene surface reflects the light emitted by one or more light sources, as seen in Figure B.2. This light passes through a group of lenses and finally reaches the sensor, which is responsible for transforming light waves into digital signals. In the industry, the most common technologies for photosensors are the CCDs (Charge Coupled Device) and the CMOS (Complementary metal-oxide Diode) but, independent on the sensor type, the image formation is never perfect. This means that there may be parts of the scene not captured and also that the image may contain distortions and noise. For this reason it is necessary to process the images in order to extract information in a more robust way [Szeliski, 2010].

B.1.1 Image Processing

As said before, the image formation is never perfect. The image is captured by a sensor and sampled into pixels that represent a limited part of the scene. It is usually assigned a value between 0 – 255 for each pixel and it can also carry color information (RGB channels), which will also be measured between 0 – 255 [Nascimento, 2015a].

Due to many reasons like light fluctuations, sensor limitations and quantization

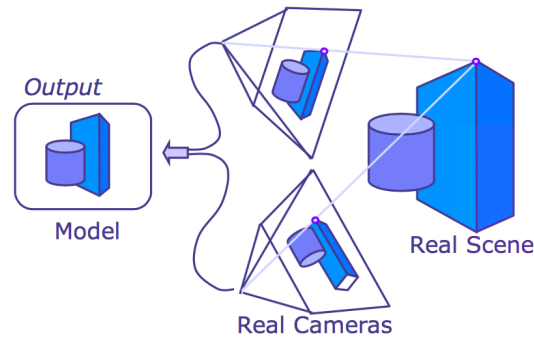


Figure B.1. Computer vision output is a model extracted from images from a real scene [Debevec et al., 2000].

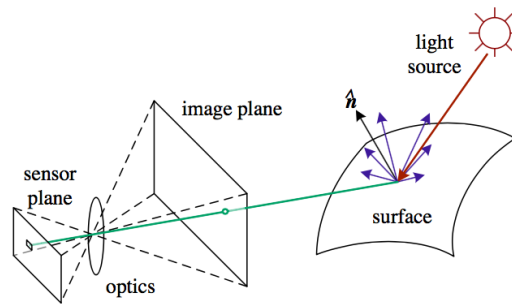


Figure B.2. The light from one or more sources is reflected by the object surface and then captured through some lens and sensor as a digital image. There are many noise sources in this process [Szeliski, 2010].

effects, images always carry noise, which are usually random fluctuations on the pixels values. This noise can be modeled as a Gaussian noise and it can be seen as the highest frequency component of the image in the frequency domain. For this reason, in order to reduce the noise effect a high frequency filter should be applied in the image, operation called “Smoothing”.

This process in the frequency domain is done multiplying the signal by the Gaussian function, which removes high frequency components from the signal. In the spatial domain (image) this process is done by Convolution operation. This operation is performed in an image using a kernel that considers the pixel neighbor value to smooth the image, removing the high frequency component.

The most used filter for removing noise is the Gaussian Smoothing [R. Fisher and Wolfart, 2016]. The kernel shown in Figure B.3 presents the 5×5 Kernel used on convolution to remove the noise from the image. Based on the 2D Gaussian function it is possible to extract the kernel, but the bigger it is the longer the calculation will take (as more neighbors are considered). For more information about convolution and

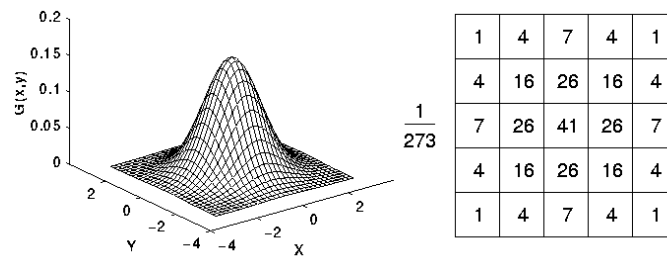


Figure B.3. 2D Gauss distribution and the 5x5 Kernel used to filter an image using Convolution [R. Fisher and Wolfart, 2016].

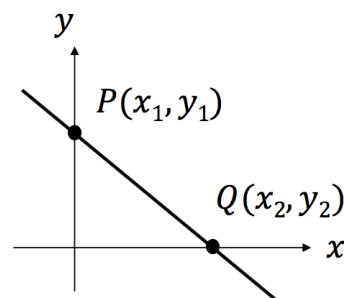


Figure B.4. Line representation in the image space [Nascimento, 2015b].

filter kernels refer to [Szeliski, 2010].

B.1.2 Hough Transform

An important feature that can be extracted from images are lines. With such information it is possible to infer the geometry of the object or even define regions of interest. The most used algorithm is the *Hough Transform* which works based on a voting procedure. The idea is to identify the line parameters with higher votes over the edges of an image [Trucco and Verri, 1998].

Before explaining the method, it is important to understand the different ways to represent a line. On the image space, a line is represented by an equation on the format $y = mx + n$, as it is possible to see in Figure B.4.

Another possible graphic representation for a line is a point in the parameter space, where the axes represent the parameters m and n of the line equation (see Figure B.5).

Consider a point in the image space; through it crosses an infinite number of lines. On the parameter space, this point can be represented as a line, where all possible values taken by m and n are represented (Figure B.6). Consider now two

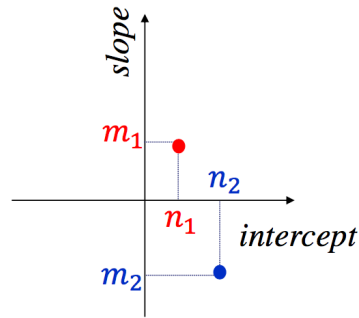


Figure B.5. Line representation in the parameter space [Nascimento, 2015b].

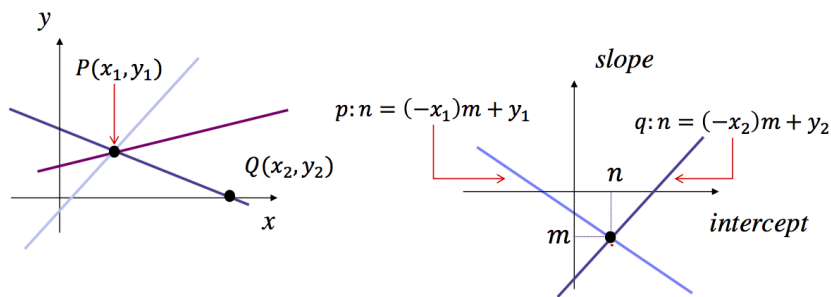


Figure B.6. In the parameter space, the crossing point indicates the equation parameters of the line that cross both points in the image space [Nascimento, 2015b].

points in the image space. As also shown in Figure B.6, the point where the lines cross in the parameters space represents the parameters of the line that cross both points in the image space.

Using some edge detection strategy (Sobel, Canny, etc), the edges in the image can be extracted. Assume now that for each pixel in the image detected as an edge, the parameters of the lines that pass through it are calculated and accumulated (voted) in a table. After doing this for all edge points, the parameters combination with higher count is the line equation that better represents the line seen in the image.

The lines are represented using the parameters ρ and θ . As it is possible to see in Figure B.7, ρ represents the distance between the line and the origin, while θ is the line orientation. Using this representation, the *Hough Transform* algorithm votes for the parameters ρ and θ with the highest counts.

The flow of the *Hough Transform* algorithm is as follow:

1. Identify image edges (Canny algorithm can be used, for example).
2. Initialize the matrix $A[\theta, \rho]$ to 0.

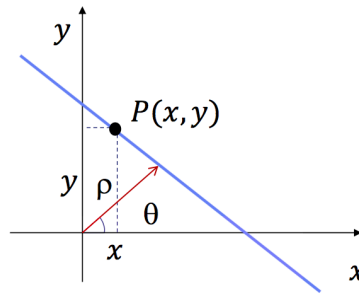


Figure B.7. Line representation in the parameter space using ρ and θ parameters [Nascimento, 2015b].

3. Discretize θ and ρ and define the increment.
4. For each pixel in the detected edges:
 - a) find the parameters θ_i and ρ_i of all lines that cross the pixel
 - b) increment $A[\theta_i, \rho_i]$
5. Find the maximum count in $A[\theta, \rho]$.

B.1.3 Optical Flow

Another interesting feature to be extracted from a group of images is the motion information. Motion can be seen in an image on three possibilities: camera still and moving scene, moving camera and scene still and also both camera and scene moving [Szeliski, 2010].

One strategy to extract the apparent motion in a scene is use brightness patterns. For this, it is assumed that the apparent brightness of a moving object remains constant. This motion estimation can be done pixel by pixel (calculating the displacement of the pixel in two frame) or looking only for visual features, like corners and textures or displacement in the images.

In both methods it is important to define the “Brightness Constancy Equation”. Consider a moving point P in a 2D scene. At time t the coordinates of P can be represented by $p = (x(t), y(t))$. Lets also express the brightness of the point P at time t as $E(x(t), y(t), t)$. Considering that an object has its brightness constant along the movement, it is possible to assume that:

$$E(x(t), y(t), t) = \text{Constant.} \quad (\text{B.1})$$

Deriving the Equation B.1 regarding time:

$$\frac{dE(x(t), y(t), t)}{dt} = 0, \quad (\text{B.2})$$

$$I_x \frac{dx}{dt} + I_y \frac{dy}{dt} + I_t = 0 \quad (\text{B.3})$$

where I_x , I_y and I_t represents the brightness derivative regarding the x axis, the y axis and time, respectively.

The Equation B.3 can be written in the matrix form

$$(\Delta E)^T \cdot v + E_t = 0 \quad (\text{B.4})$$

where:

$$\begin{aligned} \Delta E &= \begin{bmatrix} I_x \\ I_y \end{bmatrix} \Rightarrow \text{Spatial Gradient} \\ v &= \begin{bmatrix} \frac{dx}{dt} \\ \frac{dy}{dt} \end{bmatrix} \Rightarrow \text{Optical Flow} \\ E_t &= I_t \Rightarrow \text{Brightness derivative across frames.} \end{aligned}$$

Both I_x and I_y can be calculated deriving the image brightness in both x and y while I_t is obtained calculating the brightness difference of the image between frames (t). But there are still two unknowns ($\frac{dx}{dt}$ and $\frac{dy}{dt}$) so this equation is not solvable. This is known as the Aperture problem.

The Aperture problem is related to the fact that the only optical flow component that can only be estimated is the one in the same direction of the image gradient. The Figure B.8 shows a classic example of the aperture problem. The optical flow can only be estimated in the perpendicular direction of the edges. So any movement on the parallel direction won't be observed [Nascimento, 2015c].

So, in order to solve the Equation B.4, each algorithm must add some additional constraint. In this project is used the *Horn-Schunck* method, which introduces the global smoothness feature to solve the equations [Horn and Schunck, 1981].

B.1.3.1 *Horn-Schunck* Method

As said before, each optical flow method establishes another constrain to solve Equation B.4. The *Horn-Schunck* method assumes smoothness in the flow of the image to solve the problem. In other words, it looks for solutions with smaller distortions, meaning

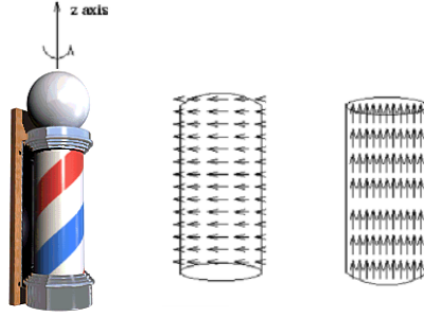


Figure B.8. Classic example of the Aperture problem. Though the lantern is spinning in the z axis the optical flow appearance is from bottom to top [Nascimento, 2015c].

more smooth flows. Thus, the method defines the Energy function as seen in Equation B.5 and tries to minimize it [Horn and Schunck, 1981].

$$E = \int \int [(I_x u + I_y v + I_t)^2 + \lambda((u_x^2 + u_y^2) + (v_x^2 + v_y^2))] dx dy. \quad (\text{B.5})$$

The first term of the equation is the one presented before in Equation B.4 (where I_x , I_y and I_t represents the derivative of the brightness E regarding x , y and t , respectively). The second term represents the smoothness of the image, where λ is a regularization constant and u_x , u_y , v_x and v_y are the optical flow components. The higher the value of λ the smoother the flow. Differentiating the Equation B.5 regarding u and v :

$$\begin{aligned} \frac{\delta E}{\delta u} &= 2I_x(I_x u + I_y v + I_t) + 2(u_{xx} + u_{yy}) \\ \frac{\delta E}{\delta v} &= 2I_y(I_x u + I_y v + I_t) + 2(v_{xx} + v_{yy}), \end{aligned}$$

where $2(u_{xx} + u_{yy})$ is the Laplacian of u and $2(v_{xx} + v_{yy})$ is the Laplacian of v . Considering the brightness constancy, the equation can be rewritten as follows:

$$\begin{aligned} I_x(I_x u + I_y v + I_t) + \nabla^2 u &= 0 \\ I_y(I_x u + I_y v + I_t) + \nabla^2 v &= 0. \end{aligned}$$

The Laplacian is related to the smoothness of the optical flow and can be simplified by $\nabla^2 u = \lambda(u - v_{avg})$ and $\nabla^2 v = \lambda(v - u_{avg})$, where u_{avg} and v_{avg} are the flow

average calculated in the neighborhood. Thus:

$$\begin{aligned} u(\lambda + I_x^2) + vI_xI_y + I_xI_t - \lambda u_{avg} &= 0 \\ v(\lambda + I_y^2) + uI_xI_y + I_xI_t - \lambda v_{avg} &= 0. \end{aligned}$$

Writing v in terms of u :

$$\begin{aligned} u &= u_{avg} - I_x \left(\frac{I_x u_{avg} + I_y v_{avg} + I_t}{I_x^2 + I_y^2 + \lambda} \right) \\ v &= v_{avg} - I_y \left(\frac{I_x u_{avg} + I_y v_{avg} + I_t}{I_x^2 + I_y^2 + \lambda} \right). \end{aligned}$$

Finally, based on these equations, the *Horn-Shunck* algorithm proposes the following interactive method to find the optical flow:

1. Calculate I_x , I_y and I_t of the image
2. For each pixel, start with $u = 0$, $v = 0$ and $n = 1$
3. Calculate u_{avg} and v_{avg} in a predefined neighborhood
4. Until $n \neq$ total iterations
 - a) $\alpha = \frac{I_x u_{avg} + I_y v_{avg} + I_t}{I_x^2 + I_y^2 + \lambda}$
 - b) $u^{n+1} = u_{avg}^n - \alpha I_x$
 - c) $v^{n+1} = v_{avg}^n - \alpha I_y$

After all iterations the value for \vec{V} are calculated.

B.2 Magnetic Field

The studies of the magnetic fields made possible to construct electric engines, water power plants and many other advances that the current society can benefit of [Halliday et al., 1992].

Differently from the electric charge, the magnetic charge cannot be found separately, meaning that it is not possible to find a positive pole without the negative one. Opposite poles attract while equal poles repel each other. Considering a magnetic bar where the poles are on the extremities, it is possible to verify the distribution of the magnetic field B going from the North pole to the South pole, as seen in Figure B.9.

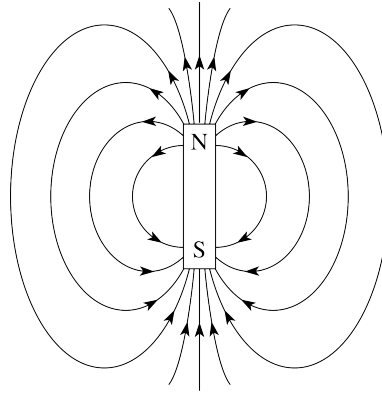


Figure B.9. Magnetic Field distribution going from the North to the South pole [Halliday et al., 1992].

B.2.1 Biot-Savart Law

In 1820, during an experiment, Hans Christian Oersted noted that electric currents create magnetic fields around a wire, and that the direction of this current also affects the direction of the magnetic field [Halliday et al., 1992]. By this experiment it was obtained the *Bio-Savart Law* that is expressed by Equation B.6.

$$dB = \frac{\mu_0 i_{ds} \sin\theta}{4\pi r^2}, \quad (\text{B.6})$$

where μ_0 is the vacuum permittivity, i_{ds} is current element, r is distance from the wire to the point and θ it the angle between ds and r (see Figure B.10).

This law can be applied to a long and straight wire and also to a coil conducting current. Consider a coil conduction current, the magnetic field on P next to the coil is expressed by Equation B.7.

$$B = \frac{\mu_0 i R^2}{2(R^2 + z^2)^{3/2}}, \quad (\text{B.7})$$

where μ_0 is the vacuum permittivity, i is the current applied to the coil, R is the coil radius and z is the distance between the center of the coil and the point P . Figure B.11 shows the magnetic field distribution and the variables involved.

From the Equation B.7 it is possible to see that the magnetic field value decreases with the distance from the coil to the point P and that it is proportional to the current applied to the coil. This information will be useful in the experiments.

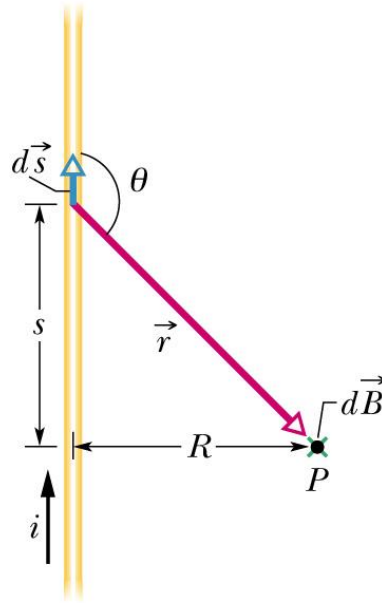


Figure B.10. *Biot-Savart Law* applied to a wire [Halliday et al., 1992].

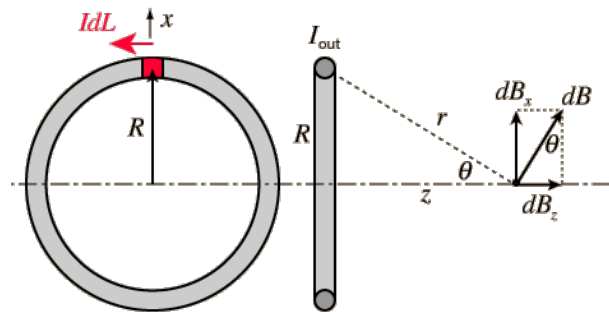


Figure B.11. *Biot-Savart Law* applied to a coil (adapted from [University, 2016]).

B.3 Quadratic-Chi Histogram Distance

One of the most used tools on image processing algorithms is the histogram. It is a graphical representation of the distribution of numerical data over some bins. They can be used to represent in an image the presence of some pixel or feature over the x axes, for example. Figure B.12 shows the color distribution of the pixels in an image. The bins are defined by the value of the pixel and the more this value is identified in the image the more its frequency in the histogram.

When using histograms in data analysis, sometimes it is interesting to compare them and define a criteria to evaluate their similarity. For this reason, Pele and Werman [Pele and Werman, 2010], a method to calculate similarity based on the Chi-Squared

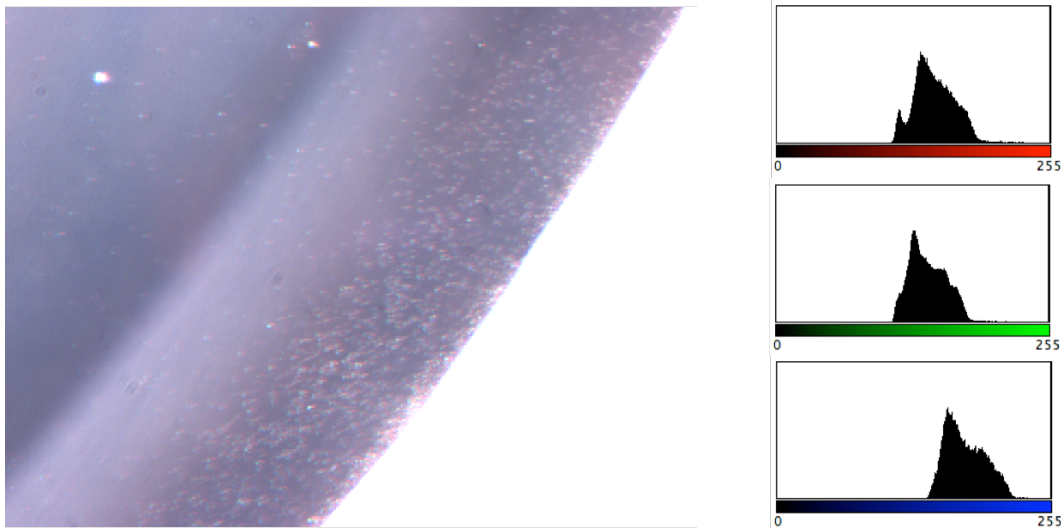


Figure B.12. RGB histogram of an image. It shows the distribution of the Red, Green and Blue values of the pixels over the image.

(χ^2) test-statistic (used to test the fitness between a distribution and observed frequencies). The method requires two histograms with the same number of bins and the general equation for the distance calculation can be seen in Equation B.8.

$$QC_m^A(P, Q) = \sqrt{\sum_{ij} \left(\frac{(P_i - Q_i)}{(\sum_C (P_C + Q_C) A_{Ci})^m} \right) \left(\frac{(P_j - Q_j)}{(\sum_C (P_C + Q_C) A_{Cj})^m} \right) A_{ij}} \quad (\text{B.8})$$

where P and Q are the two non-negative bounded histograms and A is a non-negative similarity matrix where each diagonal element is bigger or equal to every other element in its row. m is a normalization factor between 0 and 1. The distance can be implemented with the following MatLab® code.

```

1 function dist= QC(P,Q,A,m)
2     Z= (P+Q)*A;
3     % 1 can be any number as Z_i==0 iff D_i=0
4     Z(Z==0)= 1;
5     Z= Z.^m;
6     D= (P-Q) ./Z;
7     % max is redundant if A is positive-semidefinite
8     dist= sqrt( max(D*A*D', 0) );

```

According to Pele and Werman, this method was tested using a benchmark with various configurations of the Quadratic-Chi distance compared to some other distance

methods, such as "Earth Mover Distance" (EMD), L_1 norm and "Quadratic-Form". The results show that the "Quadratic-Chi" method is a good metric to evaluate the similarity between two histograms [Pele and Werman, 2010].